Bioactive Materials 38 (2024) 512–527

Contents lists available at ScienceDirect

Bioactive Materials

journal homepage: www.keaipublishing.com/en/journals/bioactive-materials

# A biomimetic tri-phasic scaffold with spatiotemporal patterns of gastrodin to regulate hierarchical tissue-based vascular regeneration

Yingrui Hu [a,b,1], Limei Li [b,1], Qing Li [b], Shilin Pan [b], Guangli Feng [c], Xiaoqian Lan [c], Jianlin Jiao [b], Lianmei Zhong [d,**], Lin Sun [a,*]

[a] Yunnan Key Laboratory of Stem Cell and Regenerative Medicine, Department of Cardiology, The Second Affiliated Hospital, Kunming Medical University, Kunming, 650101, China
[b] Yunnan Key Laboratory of Stem Cell and Regenerative Medicine, Kunming Medical University, Kunming, 650500, China
[c] Department of Neurology, The First Affiliated Hospital, Kunming Medical University, Kunming, 650032, China
[d] Department of Neurology, Xuanwu Hospital, Capital Medical University, Beijing, 100053, China

ARTICLE INFO

*Keywords:*
Tri-phasic structure
Hierarchical release of gastrodin
Anti-coagulation
Intimal hyperplasia
Regeneration

ABSTRACT

Clinical use of small-diameter vascular grafts remains a challenging issue in neovessel regeneration in view of thrombosis and intimal hyperplasia. Developing a vascular graft with structure and function similar to those of the native vessels necessitates a major direction of vascular tissue regeneration. Thus, this study sought to design and fabricate a range of tri-phasic scaffolds (0, 2, and 5 wt% gastrodin-polyurethane (PU)) with spatiotemporally defined structure and gastrodin-release for regulating the highly coordinated processes in growth of the intima and media. While the small pores of inner layer guided infiltration of human umbilical vein endothelial cells (HUVECs), the bigger pores of medial layer could offer smooth muscle cell (SMC)-friendly habitat, and external fibers conferred adequate mechanical properties. Correspondingly, spatial distribution and differential regulation of key proteins in HUVECs and SMCs were mediated by hierarchical release of gastrodin, of which rapid release in inner layer elicited enhanced HUVEC proliferation and migration against those of the SMC *via* activated endothelial nitric oxide synthase (eNOS) and heat shock protein 70 (HSP70) signal. Of note, superior anti-coagulation was reflected in 2 wt% gastrodin-PU *ex vivo* extracorporeal blood circulation experiment. After *in vivo* implantation for 12 weeks, there was no formation of obvious thrombosis and intimal hyperplasia in 2 wt% gastrodin-PU. The scaffold maintained high patency and improved vascular remodeling, including the formation of thin endothelialization in lumen and dense extracellular matrix deposition in medial layer. Taken together, the results demonstrate the positive function of hierarchical releasing system that responded to tri-phasic structure, which not only suppressed intimal thickening but also tightly controlled tissue regeneration.

## 1. Introduction

Patients with severe cardiovascular disease often require bypass surgery to circumvent tissue damage. Vascular transplantation is an effective alternative to deal with its high incidence. However, the use of small-diameter (<6 mm) vascular grafts is still confronted by inferior primary and secondary patency rates, resulting from thrombosis or intimal hyperplasia (IH) [1,2]. IH is a complex process, involving that endothelial cell damage and inflammation which can lead to aberrant [3], uncontrolled migration, and proliferation of smooth muscle cell within the intimal layer of the blood vessel wall [4]. Drug-eluting stents have been advanced to treat post-angioplasty IH but in-stent restenosis still occurs [5]. Moreover, the drugs used on the stents (e.g. rapamycin, paclitaxel) merely showed a short time success. They are indiscriminately antiproliferative which heighten the risks of thrombosis and mortality [6]. Undoubtedly, maintaining or restoring the contractile phenotype of smooth muscle cell while encouraging normal endothelial cell function, is an attractive strategy for efficiently preventing vascular

Peer review under responsibility of KeAi Communications Co., Ltd.
* Corresponding author.
** Corresponding author.
*E-mail addresses:* 13888967787@163.com (L. Zhong), sunlinkm@sina.com (L. Sun).
[1] These authors contributed equally to this work.

https://doi.org/10.1016/j.bioactmat.2024.05.007
Received 27 January 2024; Received in revised form 17 April 2024; Accepted 3 May 2024

remodeling disorders. To date, there is still lack of approved therapeutics to prevent grafts from developing IH and subsequent post-surgical graft failure.

The suitable habitats for endothelial cells and smooth muscle cells can preferentially perform their respective functions [7]. Considering the hierarchical structure of the native vascular wall, designing a multi-layer bionic scaffold as a specific habitat for distinct cell types would be an attractive strategy. Since the endothelial cell has only the size of 10~30 μm, the inner layer with small pores would selectively capture only the endothelial cells, thus hindering the migration of bigger smooth muscle cells [8,9]. Meanwhile, the pore size ranging from 60–200 μm in the medial layer conforms to the standards of effective smooth muscle cells infiltration [10]. Such a design of vascular grafts also works well in the rat common carotid arteries with a smaller diameter and lower blood flow rate [11,12]. Constructing such hierarchical structure holds significant promise for highly coordinated growth of the intima and media. However, the function of the captured cells requires suitable microenvironment stimuli.

Enhancing rapid endothelialization of synthetic grafts is beneficial to antithrombogenicity [13]. This may be contributed by endothelial cells from adherence of circulating endothelial progenitor cells (EPCs), involving chemotactic effects, recruitment, and adhesion of EPCs at neovascularization sites [14]. Coating bioactive substances and covalently immobilizing cytokines on grafts may accelerate the endothelialization of synthetic grafts [15,16]; however, bioactive molecule-inspired lumen not only favored endothelial cell adhesion but also adhered to other blood cells such as platelets and white cells, which may induce thrombogenesis. Therefore, in situ endothelialization requires conjugating active ingredients that can selectively adhere to vascular cells. Gastrodin, a primary bioactive constituent of traditional Chinese herbal medicine with potential anti-coagulation and anti-inflammatory capacities [17], has long been recognized an inherent drug for therapeutic development [18,19]. Gastrodin can effectively inhibit the formation of blood clots in blood vessels and reduce the risk of thrombosis [20], and act as a dose-dependent enhancer of angiogenesis [21]. Leveraging excellent performance of polyurethane [22,23], previous study in our laboratory has developed gastrodin modified polyurethane films to affect anti-coagulation and neovascular growth, depending on the sustained release of gastrodin [20]. Subcutaneously embedded films stimulated the revascularization, attenuating the production of fibrous capsules surrounding the implants, pioneering their application in endothelialization of vascular graft. Uniquely, when used to treat smooth muscle cells, the gastrodin may inhibit the proliferation of smooth muscle cells and reduce neointimal hyperplasia [15,24], suggesting that gastrodin regulates angiogenesis in a manner dependent on dose.

The smooth muscle cells proliferate and migrate to the intima make the vascular wall thicken and the lumen narrow [25]. Starting from the use of synthetic vascular scaffolds to reduce lumen stenosis by inhibiting the excessive proliferation and migration of smooth muscle cells, it was found that smooth muscle cells can affect endothelial cells and thereby affect the re-endothelialization of blood vessels [26]. Therefore, it is desirable to further explore whether endothelial cells would have an impact on smooth muscle cells in vascular scaffolds, so as to construct a vascular scaffold that would inhibit excessive proliferation of the intimal layer. However, the previous gastrodin delivery is simple and insufficient for a complex process involving the endothelial cells and smooth muscle cells. Therefore, a hierarchical releasing system is needed. Also, the roles of spatial distribution and differential regulation of key proteins in intimal endothelial cells and medial smooth muscle cells mediated by gastrodin modified hierarchical scaffold are not well defined. Indeed, the complexity of the *in vivo* environment hinders a comprehensive investigation of the regulatory role played by sustained release and spatial distribution of gastrodin on the angiogenic microenvironment.

Here, we have constructed a tri-phasic vascular scaffold with the porous gastrodin-polyurethane (gastrodin-PU) core enabled rapid cell infiltration, while the electrospun polycaprolactone (PCL) sheath strengthened the scaffold and trapped cells upon scaffold implantation *in vivo*. Focusing on the effects of two spatiotemporal gastrodin regulations (inner and medial layers) on angiogenesis, we hypothesized that endothelialization would be enhanced by small pore and sustained-gastrodin, and inhibited by bigger pore, which introduced smooth muscle cells into lumen would inhibit angiogenesis. We found that neovascularization responded directly to dynamically sustained-release magnitude of gastrodin and was particularly sensitive to the spatial distribution of loading gastrodin. To elucidate the cellular and molecular changes upstream of the endothelialization responses to inner versus medial layers, we investigated cell viability, proliferation, gene and protein expression profiles, and the regulation mechanism between HUVECs and SMCs. Vascular scaffold implantation in a rabbit carotid artery end-to-end model particularly showed a divergent performance (Scheme 1). This work provides a foundational understanding of how gastrodin would regulate antithrombogenicity and host remodeling. It has critical implications for developing a graft of dual controlled-release drug for synergizing regenerative therapies and rehabilitation strategies.

## 2. Materials and methods

### 2.1. Study design

This study aimed to design a tri-phasic scaffold with spatiotemporally defined structure and gastrodin-release for regulating the highly coordinated processes in growth of the intima and media. First, we constructed an inner layer of small pores (fast gastrodin release) and a medial layer of large pores (slow gastrodin release) in a layer-to-layer deposited fashion, and surrounded by fibrous PCL layer. Porous structure, mechanical properties, gastrodin releasing profile and degradation *in vitro* were characterized. HUVECs and SMCs were used as *in vitro* cell models to investigate the biocompatibility and classified regulation of different layers. The *ex vivo* thrombogenicity test was conducted to understand the anti-coagulation function driven by scaffolds. The scaffolds as vascular grafts were further investigated in rabbit models of carotid artery. To elucidate the effect of HUVEC-inner layer induced microenvironment on SMC migration, a proteomic analysis on harvested supernatant from HUVEC-inner layer incubation was applied. The number of materials, cells and animals for each group were determined with statistically significance.

### 2.2. Preparation of polymers

The gastrodin/PU polymers were prepared by using in situ polymerization as described previously [20]. Briefly, 24.00 g of poly (Ɛ-caprolactone)2000 (PCL2000), 1.20 g of poly (ethylene glycol)400 (PEG400) and 7.80 g of isophorone diisocyanate (IPDI) were mixed in a 250 mL three-necked flask under nitrogen atmosphere, heated at 70 °C with thorough stirring for 5 h to obtain the prepolymer. Then 3.70 g of Lysine ethyl ester dihydrochloride (Lys·OEt–2HCl) was used to extend the prepolymer. After stirring for 2 h, gastrodin with special content (0, 2, and 5 wt%) was added. The resultant polymer was cured at 90 °C for 6 h for subsequent use. The structure and composition of polymers were shown in Fig. S1 and Table S1.

### 2.3. Generation of gastrodin gradients using tri-phasic structure

One polymer with two conditions (small or larger pore-forming particles) was performed by a solvent casting/salt-leaching process. Dissolved gastrodin/PU in trifluoroethanol (solution I) was homogeneously cast into Teflon mold to fabricate a 2-mm-thick small pored inner layer (film). Another class of larger pored medial layer was created using a 1:2 mixture of material: sodium chloride salts by weight (solution II). The particles were leached out by washing extensively in dd$H_2O$

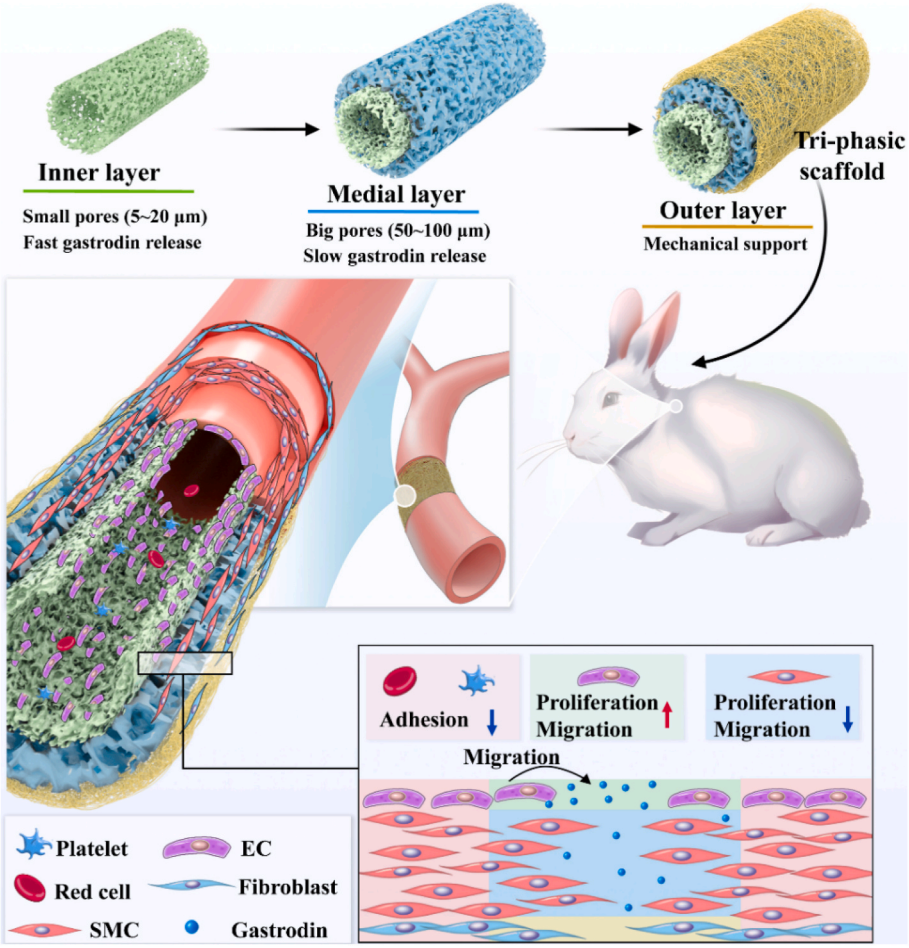


**Scheme 1.** Schematic representation of tri-phasic structure for vascular-mimic hierarchy and the classified effect of controlled-release gastrodin on endothelial cell and smooth muscle cell to regenerate vascular tissue.

for 48 h before drying at constant weight under vacuum. Heterogeneous porous layers (inner and medial layers) were developed respectively using two independent solution systems of polymer.

The strategy used for the hollow lumen formation was through the deposition of layers around a stainless steel (Ø 1.2 mm) mandrel, which could later be mechanically removed. The remaining cylindrical structure would have an emptied centric region mimicking the luminal part of vascular vessels. To fabricate multilayer cylindrical construct with different pores, a layer-by-layer dipping rounds at a defined dipping speed were performed. The first round consisted of 1 dipping in solution I (gradient I), whereas the successive rounds were 3 dippings in solution II (gradient II), followed by immersing in $ddH_2O$ for 48 h for particles removal, and finally electrospun poly (Ɛ-caprolactone)80,000 (PCL80000) as sheath. For PU, the solution I and II had same PU polymer. Similarly, 2 wt% gastrodin-PU and 5 wt% gastrodin-PU were fabricated. The obtained tri-phasic scaffold with spatial gradient of gastrodin was named as PU, 2 wt% gastrodin/PU, and 5 wt% gastrodin/PU.

### 2.4. Scaffold characterization

The morphology of tri-phasic scaffolds was characterized by scanning electron microscopy (SEM) (Regulus8100, Hitachi, Japan) at an accelerating voltage of 10 KV. Before observation, the samples were sectioned transversely and then sputter coated with gold to a thickness of around 7 nm. Micro computed tomography (Micro-CT) (NMC-200, Ping Sheng Medical Technology (Kunshan) Co, Ltd., China) was applied to reconstructed hierarchical 3D structure at a resolution of 0.008 mm with a voltage of 60 kV and a current of 0.12 mA. The volume of interest was set as a cylinder (Ø 1.2 mm × 10 mm), then analyzed by Feldkamp, Davis and Kress (FDK) algorithm.

### 2.5. Mechanical properties

The tri-phasic scaffolds with a diameter of 1.2 mm and a length of 40 mm were subjected to a tensile test using a mechanical testing instrument (CMT6103, MTS, USA). The scaffolds were tightly fixed to two clamps with a 30 mm working distance, and then stretched at a constant rate of 50 mm/min until rupture. Tensile strength and elongation at break were calculated. The tensile strength was set as the peak stress of the stress-strain curve.

Burst pressure was measured using a home-made pressurization equipment (ZC-400, Jinhu Changtong Measurement and Control Instrument Factory, China), which was assembled with a pressure gauge and an injector, according to a previous report [27,28]. In brief, the tubular scaffold (Ø 1.2 mm × 15 mm) was clamped one end and hermetically sealed the other end to a vascular catheter. $ddH_2O$ in the injector was injected into the tubular scaffold at a rate of 6 mL/min and the filling pressure was recorded at the point of sudden failure. In the light of international standard ISO 7198, the water permeability of vascular prosthesis is the water flow rate passing through the unit area of sample in unit time under the lumen liquid pressure of 120 mmHg [29]. Herein, the filling pressure in the sample was held for 1 min at 16 kPa, and water seeping through the wall of sample was weighed. At least five specimens were tested for each sample. The water permeability was calculated according to the following equation:

$$\text{water permeability} = \frac{V_l}{S_s}$$

$$S_s = \pi D_s \times L_s$$

Where $V_l$ is the volume of leaked water, $S_s$ represents the lumen area of the prepared sample, $D_s$ and $L_s$ represent the lumen inner diameter and the length of the sample, respectively.

### 2.6. Tailoring the gastrodin release profile of tri-phasic scaffolds

To investigate whether the addition of particles can tailor the gastrodin release profile over a long culture period, three types of samples were tested and compared: inner layer, medial layer (Ø 13 mm × 2 mm) and tri-phasic scaffold (Ø 1.2 mm × 10 mm). These samples were cultured in 1.5 mL NaOH solutions in 37 °C water bath shaking for up to 12 weeks and media from each sample were changed weekly. For gastrodin release study, medium samples were taken weekly and analyzed using high performance liquid chromatography (Hitachi L - 2000, HITACHI, Japan). For the degradation study, samples were washed and dried at 40 °C and each time point (weeks 3/7, 1, 2, 4, 8, and 12). Each sample was then weighed using an analytical balance (Mettler Toledo, USA).

### 2.7. Cell culture

HUVECs and SMCs were obtained from BeNa Culture Collection Co., Ltd (BNCC, China). Both cells were cultured in dulbecco's modified eagle medium/nutrient mixture F-12 (DMEM/F12) medium (Corning, USA) supplemented with 10 % fetal bovine serum (FBS) (Gibco, USA), 1 % penicillin-streptomycin (HyClone, USA) in a humidified incubator (37 °C, 5 % $CO_2$), and the media was changed every other day. Layers (Ø 13 mm × 2 mm) were sterilization with γ-ray irradiation with 15 kGy before incubated overnight in well plates using DMEM/F12 media, and then seeded with cells.

For the inner layer (gradient I) study, the HUVECs were seeded ($1.5 \times 10^4$ cells/cm$^2$) onto each inner layer and cultured for a period of 5 days. The media incubated for 3 days was collected to obtain the supernatant as the conditioned media for subsequent experiments. To determine the interaction of cell-medial layer (gradient II), SMCs were seeded at the density of $0.5 \times 10^4$ cells/cm$^2$ on the layers. Cell counting kit-8 (CCK-8) (#CK04, Dojindo, Japan) was used to evaluate proliferation of cells after culture of 1, 3, and 5 days. 5-ethynyl-2′-deoxyuridine (EdU) (#C0075S, Beyotime, China) staining was also performed at predetermined time points. Cell viability was determined using Live/Dead Viability/Cytotoxicity Kit (#B34954, Life Technologies, USA). Immunofluorescent staining was performed using anti-α-smooth muscle actin (α-SMA), Osteopontin for SMCs. The related expression of genes and proteins (vascular endothelial growth factor (VEGF), VE-cadherin, and eNOS for HUVECs; α-SMA, calponin, and osteopontin for SMCs) were assessed by reverse transcription and quantitative polymerase chain reaction (RT-qPCR) and Western blotting (WB), respectively. The level of eNOS was also analyzed by ELISA kit (Shanghai Enzyme-linked Biotechnology Co., Ltd, China) according to the manufacturer's instructions.

Migration of HUVECs and SMCs: Cells were seeded on the surfaces of the layers in 6-well plates, respectively. At the predetermined intervals, a scratch was made using a sterile 200-μL pipette tip, and cell debris was washed with phosphate buffer saline (PBS). The media without FBS was then added to the wells. Cell migration propensity was imaged and the wound areas were measured by Image Pro Plus v6.0. Herein, HUVEC-inner layer incubated for 0, 12, 24, 48, and 72 h, whereas SMC-medial layer was at 0, 6, 12, 24, and 48 h.

Tube formation assay: HUVECs at a density of $6 \times 10^4$ cells/well were seeded onto 48-well plate coated with 100 μL Matrigel (#356234, BD, USA), followed by addition of conditioned media that supernatant of co-cultured HUVEC-inner layer was 2-fold diluted with fresh DMEM/F12. After incubation for 6 h, tubes were photographed and the number of segments, length and connections were counted using Image J.

### 2.8. Classified regulation of different cells by heterogeneous porous layers

To confirm that HUVEC-inner layer could affect SMC, SMCs ($6 \times 10^3$ cells) were seeded into the upper transwell inserts with polycarbonate membrane pore size of 8 μm (Corning, USA) whereas HUVECs ($2 \times 10^4$ cells)-inner layer in the lower 24-well plates. The effects of SMCs ($1 \times 10^4$ cells)-medial layer on HUVECs ($1.2 \times 10^4$ cells) were similarly designed. After 1 and 3 days of incubation, the cells in the upper chamber were fixed and stained with crystal violet (#G1062, Solarbio, China).

A special culture medium for SMCs was prepared by 2-fold dilution of aforementioned HUVEC-inner layer conditioned medium with fresh DMEM/F12. SMCs were seeded onto medial layers and cultured in special medium. The proliferation of cells was assessed using CCK-8 after 1, 3, and 5 days. The cell samples were harvested at 3 days and analyzed protein (HSP70, calponin, osteopontin) expression by WB. Furthermore, the proliferation of HUVECs incubated in the SMC-medial layer conditioned medium with fresh DMEM/F12 at a ratio of 1:1 was detected at 1, 3, and 5 days.

The aforementioned supernatant of co-cultured HUVEC-inner layer was collected and then frozen at −80 °C. The proteomic analysis was performed at Beijing Novogene Biotech. The Kyoto Encyclopedia of Genes and Genomes (KEGG) database and biological process enrichment analyses of differentially expressed proteins were performed. The interaction network analysis was visualized by STRING (STRING; https://www.rcsb.org/). For molecular docking, the 3D structures of eNOS and HSP70 were obtained from the PDB database (https://www.rcsb.org/). After removed water molecules, server provided by the Center for Computational Biology at the University of Kansas and the software programs (PyMOL and Maestro) was applied to predict molecular docking. Co-immunoprecipitation (Co-IP) assay was performed to detect the interaction between eNOS and HSP70.

### 2.9. Ex vivo anti-coagulation response of tri-phasic scaffold

3 New Zealand white rabbits (2.5–3.0 kg) were used for *ex vivo* thrombogenicity test. All animal experimental protocols followed the guidelines and regulations of the Institutional Animal Care and Use Committee of Kunming Medical University (China). After general anesthesia by 3 % pentobarbital sodium salt (30 mg/kg), the left carotid artery and the right jugular vein of the rabbit were separated and then connected with a commercially available polyvinyl chloride (PVC) cardiopulmonary perfusion tubing. The PU, 2 and 5 wt% gastrodin-PU tri-phasic scaffolds (Ø 5 mm × 40 mm) were wrapped around the outer wall of PVC tubes. 0.9 % sodium chloride solution was supplemented during the experiment. After 2 h of blood circulation, the samples were removed from the circulation system for photographing and fixed with 3 vol% glutaraldehyde. The cross section of the scaffold was photographed to analyze the occlusion rate. Prior to SEM observation, the samples were rinsed with PBS, dehydrated through graded ethanol and dried.

The rabbit blood was collected in anti-coagulant tube and centrifuged at 250 g for 15 min to obtain platelet-rich plasma (PRP). The tri-phasic scaffold (Ø 1.2 mm × 10 mm, n = 5) were rinsed with PBS and then immersed in PRP for 3 h at 37 °C to allow interaction between the PRP and scaffolds. After that, the scaffolds were washed repeatedly with PBS to remove the unadhered platelets and then fixed with 3 vol% glutaraldehyde for SEM observation.

### 2.10. In vivo implantation evaluation on rabbit carotid artery model

The scaffold implantation involved 30 New Zealand white rabbits

with weight ranging from 2.5 to 3.0 kg. Rabbits were divided into three groups: PU, 2 and 5 wt% gastrodin-PU. After general anesthesia, the hair around the neck was shaved and then the rabbits were gently fixed on an operation table. The right internal carotid artery was exposed fully and a defect of 5-mm length was transected between the clamp under a surgical microscope. Auricular vein was given continuous drip 0.9 % sodium chloride solution during the experiment. Before implanted into the defect, a sterilized scaffold (Ø 1.2 mm × 10 mm) was immersed in heparin sodium saline for 2 h, then sutured using end-to-end anastomosis (12-0 surgical suture) after the anastomotic site was rinsed with heparin sodium saline. The musculature and skin incision then closed with absorbable sutures (4-0 surgical suture). Finally, anti-inflammatory using antibiotics and systemic anticoagulant therapy using heparin sodium lasted for 3 days after scaffold implantation.

Doppler ultrasound assessment was performed on rabbits implanted with tri-phasic scaffolds at 1, 3, 5 and 7 weeks using an ultrasound imaging system for small animals (VINNO, China). Before ultrasonic evaluation, the rabbits were anesthetized and had hair around the neck cleaned. The color mode and pulse wave mode were used to evaluate the patency, and flow velocities.

The rabbits were euthanized at postoperative weeks 4 and 12, and the arteries with implantations were harvested and gently washed with heparinized saline. Collected blood serum was assayed to measure the content of tumor necrosis factor-α (TNF-α) using related ELISA kit. The extract samples were fixed with 4 % paraformaldehyde solution for 7 days, dehydrated through gradient saccharose, and then embedded in optimal cutting temperature compound (OCT) (Thermo Fisher Scientific, America). Consecutive 6–8 μm sections in a longitudinal and transverse way were cut by a freezing microtome (Thermo Fisher Scientific, America). For histological hematoxylin-eosin (H&E) staining (#G1120, Solarbio, China), the occlusion rate was calculated by measuring the cross-sectional area of the lumen at least five different samples for each group.

For immunofluorescence staining, longitudinal sections were permeabilized in PBS/Triton x-100 (0.5 %) for 20 min, blocked with 10 % goat serum in PBS solution for 3 h, following exposure to primary antibody overnight at 4 °C. The primary antibodies, each used at 1:100 dilution, were as follows: collagen I, cocktails (Platelet endothelial cell adhesion molecule-1 (CD31) and α-SMA, Arginase-1 (Arg-1) (M2 marker) and TNF-α (M1 marker)). After again washed with 0.05 %

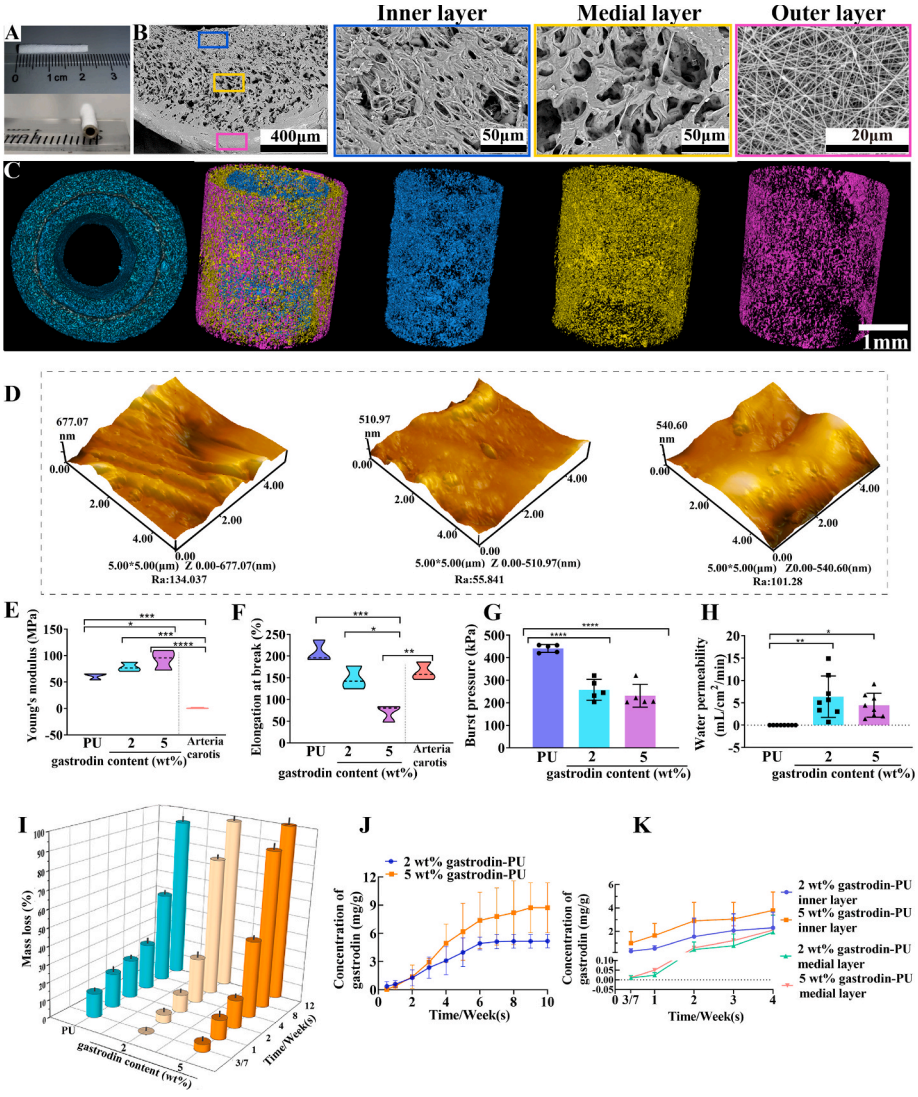


**Fig. 1.** Characterization of tri-phasic gastrodin/PU scaffolds. (**A**) The visualized vascular scaffolds. (**B**) Macrostructure of gastrodin/PU scaffolds was observed by SEM. (**C**) 3D micro-CT reconstruction models of hierarchical structure. (**D**) The roughness of inner surface by AFM. (**E–H**) Mechanical properties including (**E**) Young's modulus (n = 3), (**F**) Elongation at break (n = 3), (**G**) Burst pressure (n = 5), and (**H**) Water permeability (n = 8). (**I**) Mass loss of tri-phasic scaffold in 0.1 M NaOH liquid, and (**J**) cumulative release of gastrodin (n = 3). (**K**) Cumulative release of gastrodin of the fast release in inner layer versus the slow release in medial layer (n = 3). ****$P < 0.0001$, ***$P < 0.001$, **$P < 0.01$ and *$P < 0.05$ by one-way ANOVA with Tukey correction.

Phosphate buffered saline with tween (PBST), the specimens were incubated with secondary antibody cocktails for 2 h at room temperature, and then counterstained with 4′,6-diamidino-2-phenylindole (DAPI) (#d9542, Sigma-Aldrich, USA). Tables S3 and S4 listed the antibodies used for immunofluorescence. In the case of morphological changes of the scaffold, the cross-sectional structure was observed by SEM.

### 2.11. Statistical analysis

Results were expressed as means ± SD. When there were more than two groups and one time point, a one-way analysis of variance (ANOVA) was performed. All statistical analyses were performed using GraphPad Prism v8.0. Statistical significance was accepted at $P < 0.05$.

## 3. Results

### 3.1. Fabrication and characterization of gastrodin/PU tri-phasic scaffold

In our previous study, we designed PU with appropriate contents of gastrodin to make the elastomer. Here, we further developed a tri-phasic structure with gastrodin gradient distribution (Fig. 1A). To demonstrate the utility of the bi-phasic structure, layer-to-layer deposit was used to generate a spatial gradient of gastrodin center *via* structural control, as it substantially increased the construct hierarchy while allowing divergent layers of material to be orderly deposited. Homogenous polymer mixture was used to construct an inner layer of small pores with a medial layer of large pores around the core. Three different types of vascular scaffolds were made with the same design of a tri-phasic structure: an inner layer of smaller porous polymer and a medial layer of bigger porous polymer center, as well as outer layer of fibrous PCL periphery (Fig. 1B). SEM showed a highly gradient porous center in a cross-sectional view, wherein the inner layer had pore size range of 5∼20 μm and medial layer was 50∼100 μm. The inner diameter of the scaffolds was 1.20 mm, with a 150–200 μm thick of inner layer, a 300–400 μm thick of medial layer, and a 40 μm thick of dense electrospun PCL sheath. Micro-CT examination exhibited distinct three hierarchies.

(Fig. 1C). As shown by AFM, smoothness of inner surface in 2 and 5 wt% gastrodin-PU was slightly superior to PU (Fig. 1D).

The tensile properties of the tri-phasic scaffolds with various gastrodin content were calculated from stress-strain curves. The data showed that Young's modulus of the PU, 2 and 5 wt% gastrodin-PU were (61.52 ± 6.34) MPa, (78.29 ± 8.64) MPa, and (92.84 ± 18.744) MPa (Fig. 1E), respectively, which were higher than native carotid arteries of rabbit ((0.96 ± 1.14) MPa). Gastrodin content had an intense effect on the tensile properties of the scaffolds. Nonetheless, increases in gastrodin content significantly reduced the ultimate maximum load (elongation at break, $P < 0.05$, Fig. 1F). Obviously, ultimate maximum load of 2 wt% gastrodin-PU and native carotid arteries was equivalent. Although burst pressure of gastrodin-PU was significantly lower that of PU, 2 wt% gastrodin-PU had the closest resemblance to the burst pressure of the human saphenous vein (180–260 kPa) through the burst pressure instrument detection (Fig. 1G). All types of tri-phasic scaffold effectively increased burst pressure beyond that of bi-phasic scaffold (Fig. S4), which were ascribed to the electrospun PCL sheath. Water permeability analysis revealed that completely sealed tube walls were obtained in PU, while higher 2 wt% gastrodin-PU (6.35 ± 4.63) and 5 wt% gastrodin-PU (4.45 ± 2.69) was found, demonstrating moderate benefit to effective information exchange within the microenvironment (Fig. 1H).

For synergistic release of gastrodin, scaffolds were incubated in 0.1 M NaOH solution. Both 2 and 5 wt% gastrodin-PU groups showed a similar sequential gastrodin release profiles over the first 6 weeks. After this, there was a difference in which 5 wt% gastrodin-PU accelerated the gastrodin release when compared with 2 wt% gastrodin-PU, which lasted until the tenth week (Fig. 1J). The degradation rate of the scaffolds was also investigated. The mass loss presented was significantly increased over a prolonged duration (Fig. 1I). Degradation accelerated significantly at 4 weeks in all three types of scaffolds, peaking at 8 weeks. All scaffolds disintegrated at the end of 12 weeks, and the residuum was hardly distinguishable. Compared to PU group, 2 and 5 wt % gastrodin-PU groups exhibited higher degradation rates, which, in turn, increased gastrodin release.

To establish whether the addition of pore-forming particles to the polymer could further tailor gastrodin release profile of polymer due to their different pores and density, inner and medial layers were respectively cultured in 0.1 M NaOH (Fig. 1K). Faster gastrodin release was concentrated in inner layers, of which 5 wt% gastrodin-PU was higher than 2 wt% gastrodin-PU group, suggesting that the release may be attributed to proportion of gastrodin mass per unit volume. Although lower than inner layers, the slow gastrodin release in medial layers exhibited a similar expression pattern. The addition of pore-forming particles markedly slowed the *in vitro* release of gastrodin from medial layer, resulting in a reasonable constant release of gastrodin. It is notable that release rate of gastrodin in inner layer was rapid at initial stage and then tended to slow down (Fig. S6). By contrast, release rate of gastrodin in medial layer showed a slow upward trend, but was always lower than that in the inner layer. These results indicated that spatial gradients of gastrodin, coupled with temporally distinct gastrodin release profiles spanning from days to weeks, were achieved and as a candidate scaffold.

### 3.2. SMC growth controlled by larger pored gastrodin/PU medial layer

Graft implantation usually causes endothelium damage, which inevitably leads to the leak of smooth muscle cells. Thus, the growth and migration behaviors of SMCs on different medial layers were first investigated. As shown in (Fig. 2A and B), all the groups had same adhesion and proliferation of SMCs after 1-day culture. Compared to PU group, gastrodin-PU groups showed significant inhibition on SMCs, although continuous growth was still maintained over the extended period, indicating that the gastrodin-releasing property is crucial for inhibiting SMCs excessive growth. To confirm the reduction of SMCs was also reflected in their migration behavior, the migration distances of SMCs on different layers were recorded. The migration of SMCs on all substrates was increased with the extension of culture time (Fig. 2C). Upon the addition of sustained-release gastrodin, the properties of cell migration on the medial layers were remarkably restricted. Among them, the SMC migration distance in the gastrodin-PU showed the most substantial decrease of 32.0 % and 46.8 % compared with the PU after 6 and 12 h of culture, respectively. The wound-healing rate of SMCs in 2 wt% gastrodin-PU was lower than that of the PU at 24 and 48 h(Fig. 2D). In the late stage of development, 5 wt% gastrodin-PU maintained its downward trend and exerted a more significant reduction effect on wound-healing rate at 48 h.

To elucidate the underlying phenotypic changes of SMCs, we detected the mRNA expression level of related markers. As shown by RT-qPCR (Fig. 2E), α-SMA and osteopontin genes were enriched in 2 wt% gastrodin-PU after 3- and 5-day culture. They were significantly higher than that in both PU and 5 wt% gastrodin-PU groups. Likewise, α-SMA and osteopontin expression was detected by immunofluorescence (Fig. 2G), suggesting that the better SMC inhibition effect of the 2 wt% gastrodin-PU may be attributed to optimal gastrodin release in the local microenvironment. The significant difference appeared to be pronounced throughout the 5-day incubation period. A similar protein trend in protein expression changes was observed in WB analysis at day 3 (Fig. 2F).

### 3.3. HUVEC growth promoted by small pored gastrodin/PU inner layer

In addition to investigate the effect of gastrodin-releasing medial layer on SMC inhibition, the effect of inner layer on HUVEC is also important because of its correlation to endothelial regeneration. In view of this, the HUVEC behaviors on different inner layers were also

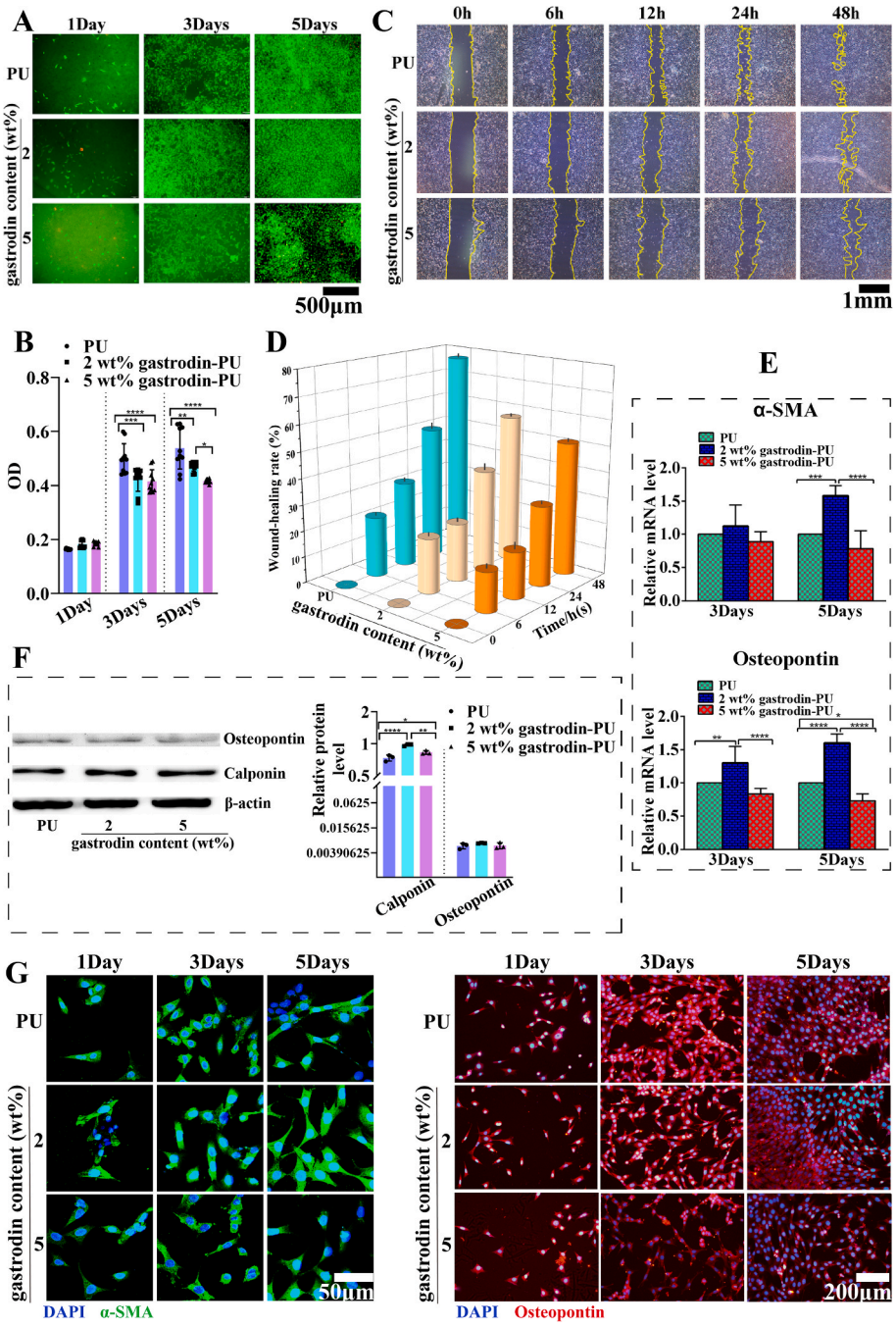


**Fig. 2.** Slow delivery of gastrodin in medial layer led to controlled SMC proliferation and migration while promoting the contractile phenotype *in vitro*. (**A**) The viability of SMCs cultured on medial layers. (**B**) Inhibited proliferation of gastrodin-PU versus PU measured by CCK-8 assay (n = 8). (**C**) A scratch test was performed to assess the migration ability of SMCs in the different groups. (**D**) The quantitative analysis of wound-healing rate (n = 3). (**E**) Expression of genes related contractile (α-SMA) and synthetic (osteopontin) markers (n = 4). (**F**) Expression of calponin and osteopontin proteins at 3 days. (**G**) IF staining of α-SMA and osteopontin. $^{****}P < 0.0001$, $^{***}P < 0.001$, $^{**}P < 0.01$ and $^{*}P < 0.05$ by one-way ANOVA with Tukey correction.

investigated. Live/Dead results (Fig. 3A) showed that cells adhered and grew on the surface of each layer on days 1 and 3, and further infiltrated into pores on day 5. Remarkably, 2 wt% gastrodin-PU layer efficiently enhanced HUVEC viability and proliferation in the presence of gastrodin loading. In contrast, dead cells (in red) were found on the PU and 5 wt% gastrodin-PU layers. CCK-8 assay showed that gastrodin-PU groups provided a better surface microenvironment for HUVEC growth (Fig. 3B). There was no significant difference in proliferation between 2 and 5 wt% gastrodin-PU groups. However, in both 2 and 5 wt% gastrodin-PU groups, the numbers of HUVECs were more than PU group (Fig. 3C). Further, the migration distances of HUVECs seeded onto gastrodin-PU were enhanced compared with PU at each pre-determined time point. As shown in Fig. 3D, the migration of HUVECs on all groups showed acceleration over time, whereas gastrodin-PU groups showed enhanced cell migration compared to PU group (Fig. 3E). The results suggested that gastrodin-PU increased the cell numbers at initial stage; meanwhile, considerable remodeling occurred in the cellular microenvironment that promoted vascular connections (Fig. 3F and G). Specifically, the angiogenic induction mainly resulted from the increased VEGF, VE-cadherin, and PDGF levels. Of note, the expression of VEGF in 2 wt% gastrodin-PU group was higher than 5 wt% gastrodin-PU group after cultured for 3 and 5 days. VE-cadherin and PDGF expression

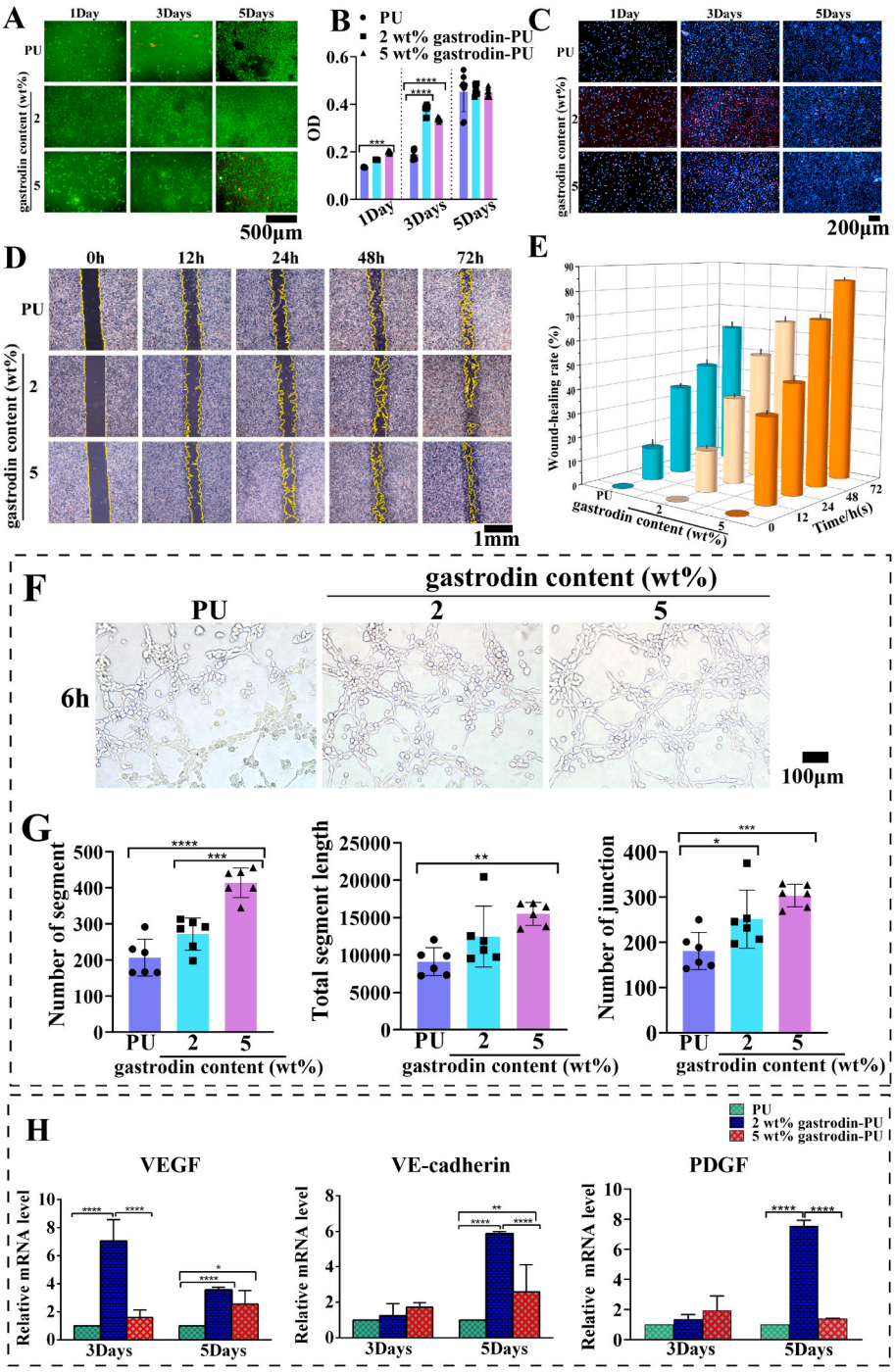


**Fig. 3.** Enhanced angiogenesis of HUVECs due to fast gastrodin release of inner layers *in vitro*. (**A**) The viability of HUVECs cultured on inner layers. (**B**) Proliferative measurement of the CCK-8 assay (n = 8). (**C**) EdU staining. (**D**) A scratch test was performed to assess the migration ability of HUVECs in the different groups. (**E**) The quantitative analysis of wound-healing rate (n = 3). (**F** and **G**) The representative pictures and quantitative estimation of the tube formation assay. (n = 6) (**H**) Expression of genes related angiogenesis (n = 4). $^{****}P < 0.0001$, $^{***}P < 0.001$, $^{**}P < 0.01$ and $^{*}P < 0.05$ by one-way ANOVA with Tukey correction.

remained relatively unchanged at day 3 but was markedly enhanced at day 5 (Fig. 3H).

### 3.4. Effects of classified controlled-release gastrodin on HUVECs and/or SMCs

To further explore the underlying mechanism and related bioevents of sustained-gastrodin induced endothelial cell infiltration, and regeneration, we performed an *in vitro* study based on co-cultures of SMCs and HUVEC-inner layer under different conditions. As shown by SMC migration in transwell (Fig. 4A), gastrodin-PU groups exerted more potent inhibitory effect on the migration of SMCs than PU group. This persisted till the third day whence the migration of SMCs on 2 wt% gastrodin-PU group was lowest in number. There was nearly 3-fold reduction compared with that in 5 wt% gastrodin-PU. Of note, the inhibitory effect of PU on migration of SMCs was the weakest. When SMCs were cultured in the conditioned medium of HUVEC-inner layer (Fig. 4C), the cell proliferation in gastrodin-PU groups was limited compared to that in the PU group; the inhibitory effect on cell growth was maintained throughout the incubation period. The results

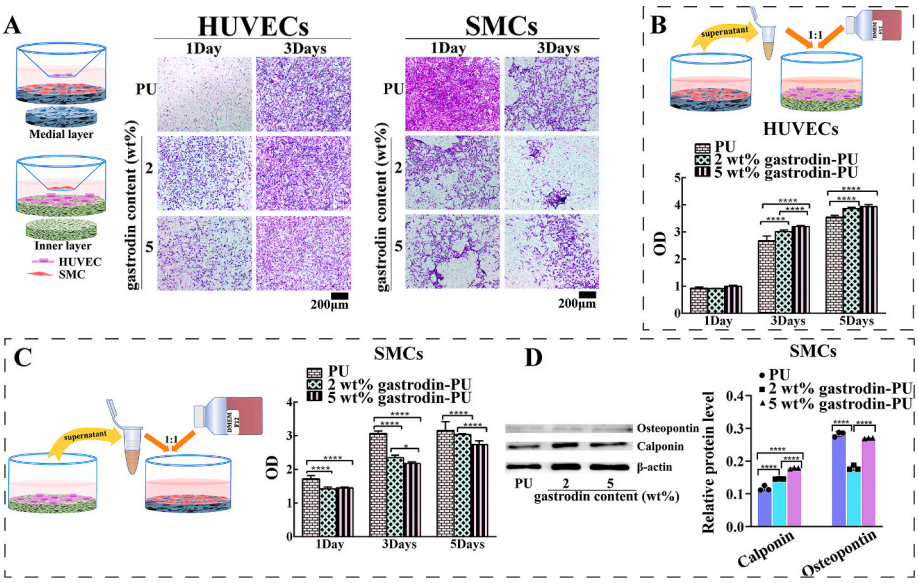


**Fig. 4.** Dual-selective regulation of HUVEC and SMC by inner or medial layers. (**A**) Transwell diagram and crystal violet staining of cell migration: HUVECs regulated by SMC-medial layer, and SMCs regulated by HUVEC-inner layer. (**B**) Proliferation of HUVECs treated with SMC-medial layer-conditioned medium (n = 8). (**C**) Proliferation (n = 8) and (**D**) protein level (n = 3) of SMCs treated with HUVEC-inner layer-conditioned medium. ****$P < 0.0001$ and *$P < 0.05$ by one-way ANOVA with Tukey correction.

necessitated the analysis of the critical factor in HUVEC-inner layer that prevented SMC excessive growth. After cultured for 3 days, 2 wt% gastrodin-PU group enhanced the expression of contractile marker (calponin) but lowered the expression of synthetic marker (osteopontin) (Fig. 4D), thus indicating its anti-proliferative effects.

Different from the result of SMC proliferation inhibited by HUVEC-inner layer, HUVECs cultured with SMC-medial layer in transwell showed the opposite trend. It is noteworthy that, there was no significant difference in migration regardless of whether the PU was incorporated with gastrodin (Fig. 4A). HUVEC proliferation, cultured in conditioned medium of SMC-medial layer (Fig. 4B), as determined *via* the CCK-8 assay, further demonstrated that the number of HUVECs in both the 2 and 5 wt% gastrodin-PU groups was markedly higher than that in PU group. This is consistent with the proliferation and infiltration results that only HUVECs had seeded onto the inner layer. Together the results underscore the importance of local gastrodin, notably of its endothelialization functions.

### 3.5. Differential protein expression and activation of HSP70 characterize the response of HUVEC to inner layer

The supernate in coculture of HUVECs and inner layer was collected at 3 days for bioinformation analysis. 300 differentially expressed proteins were identified and analysis implicated 90 meaningful proteins. KEGG pathway enrichment analysis showed that these differentially expressed proteins were enriched in some inflammatory and endothelial nitrogen oxides-related pathways, such as mitogen-activated protein kinase (MAPK) and estrogen signaling (Fig. 5B). Functional enrichment analysis showed that HSPA1B (HSP70) was mainly enriched in gastrodin-PU groups, and was more sensitive to the 2 wt% gastrodin-PU inducement (Fig. 5C). Protein interaction analysis indicated that the related proteins were mainly enriched in HSPA1B (HSP70), HSP90AA1, and NOS3 (eNOS) (Fig. 5D). It was surmised that, HSP70 and eNOS signaling may be activated, and HSP90 may act as a bridge. Consistently, molecular docking simulations predicated a bind of eNOS to HSP70 (Fig. 5E). Co-immunoprecipitation further proved that eNOS bound to HSP70 (Fig. 5F). As shown in ELISA assay, eNOS content of supernate was concentrated in both gastrodin-PU groups and suboptimal in PU (Fig. 5G). A similar eNOS expression in HUVECs was also found using WB analysis (Fig. 5H), which was markedly upregulated in 2 wt% gastrodin-PU group.

Previous studies have indicated that the HUVEC-inner layer coculture-caused inhibition of SMCs that was also reflected in their migration behavior. Therefore, to verify overexpressing eNOS secreted by HUVECs could potentiate the beneficial effects of these cells in regulating SMC function, the above-mentioned supernatant was used to treat SMCs for 3 days. As shown by WB (Fig. 5I), expression of HSP70 was significantly increased in 2 and 5 wt% gastrodin-PU groups ($p < 0.0001$), indicating the successful creation of an inhibitory microenvironment for SMCs. The regulation of HUVECs could change the pattern of cytokine production and consequently alter the microenvironment.

### 3.6. The antithrombogenic properties of tri-phasic scaffold both ex vivo and in vitro

When blood comes in contact with a foreign material, plasma proteins will adsorb onto the surface of the material, trigger platelet adhesion or aggregation. The antiplatelet properties *in vitro* showed that little platelet was observed in the gastrodin-PU groups, especially 2 wt% gastrodin-PU group. In contrast, the platelet count was remarkably increased in PU group (Fig. 6A). Furthermore, the hemolysis rate, an important parameter to measure the blood compatibility, reflects the damage caused by biomaterials on red blood cells (RBCs). As shown in Fig. 6B, the hemolysis rate of PU was much higher than the gastrodin/PU groups. It is worth noting that 2 wt% gastrodin/PU had the slowest hemolysis rate, which meets the safety range of biomaterials [30], demonstrating that a certain amount of gastrodin in PU can improve hemocompatibility. Together with hemolysis rate, activated partial plasma prothrombin time (PT), activated partial thromboplastin time (APTT), and thrombin time (TT) were used to determine the anti-coagulation activities of scaffolds (Fig. 6C and D and E). Compared with the control, PT for PU was slightly prolonged, while PT for the 2 wt % gastrodin-PU markedly increased, confirmed by a similar tendency of APTT and TT.

To verify the practical antithrombogenic efficacy, an *ex vivo* extracorporeal blood circulation experiment was further performed. PU, 2 and 5 wt% gastrodin-PU were curled up and wrapped onto a commercially available medical three-way catheter and then connected to

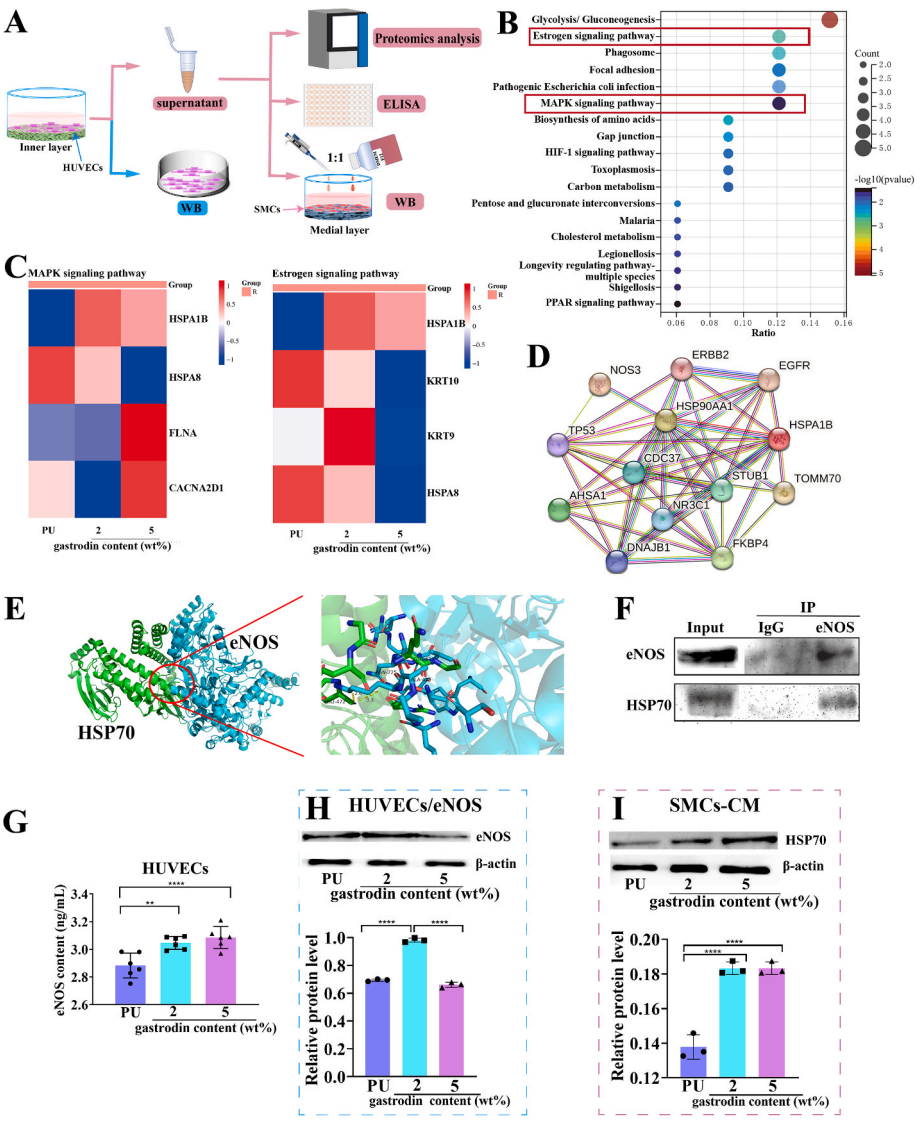


**Fig. 5.** Exploration of protein expression and functional enrichment analysis. (**A**) A schematic diagram of HUVEC-inner layer-conditioned microenvironment. (**B**) KEGG enrichment analysis and the related signaling pathways were highlighted by a red box. (**C**) Heat map showing relative protein expressions. (**D**) Interaction network of proteins HSPA1B (HSP70) and NOS3 (eNOS) involved in the conditioned medium. (**E**) Prediction of a potential interaction between eNOS (cyan) and HSP70 (green) based on molecular docking. (**F**) The interaction between eNOS and HSP70 by Co-IP assay. (**G**)The concentration of eNOS in the conditioned medium (n = 6). (**H**) Expression of eNOS in HUVECs (n = 3). (**I**) Expression of HSP70 in SMCs treated with conditioned medium (CM) (n = 3). ****$P < 0.0001$ and **$P < 0.01$ by one-way ANOVA with Tukey correction.

arteriovenous shunt circuit in a rabbit (Fig. 6F). As shown in Fig. 6G, after 2 h of *ex vivo* blood circulation, the 2 and 5 wt% gastrodin-PU groups showed better permeability and less thrombus than PU group. SEM results revealed that quantitation of RBC in the 2 wt% gastrodin-PU group was significantly reduced, followed by 5 wt% gastrodin-PU group, whereas PU had the largest amount of RBC (Fig. 6H). The findings suggest that PU incorporated opportune gastrodin can reduce thrombogenesis and improve patency.

### *3.7. Tri-phasic scaffold maintains a high patency rate and presents regeneration in rabbit carotid artery*

Since gastrodin-PU scaffold was vascular cell compatible while providing a positive regulation of localized microenvironment, their vascular repair performance was further evaluated through 12-week implantation in a rabbit carotid artery interposition model (Fig. 7A). Macroscopic images showed that the tri-phasic scaffolds had no blood leakage from the wall at time of implantation. To evaluate the patency of the scaffolds, blood flow in the right carotid artery was monitored by Doppler ultrasound at 1, 3, 5, and 7 weeks (Fig. 7B). Both PU and 5 wt% gastrodin-PU groups exhibited blood reflux at 1 week, and PU group was further aggravated at 3 weeks. In contrast, the overall patency rate for 2 wt% gastrodin-PU scaffold was maintained before sacrificing at each time point. Quantification of peak flow rate (as indicated by distance between two parallel dash lines) showed that the flow rate was increased for all the three groups at the time of implantation. From 1 to 7 weeks, significant difference in flow rate between different groups was found and the flow rates of gastrodin-PU groups were significantly higher than that of PU group. Very strikingly, the 2 wt% gastrodin-PU group presented a faster blood flow than that of the 5 wt% gastrodin-PU group, indicating that the proper spatiotemporal gastrodin was beneficial for maintaining the patency of the vascular scaffolds *in vivo*.

Next, the implanted scaffolds were harvested from the rabbits and processed for H&E staining at 4 and 12 weeks. In a cross-section (Fig. 7C and D), occlusion of PU and 5 wt% gastrodin-PU groups at 1 month was evident. The middle thrombus ratio (43.97 ± 5.256 %) of cross sections

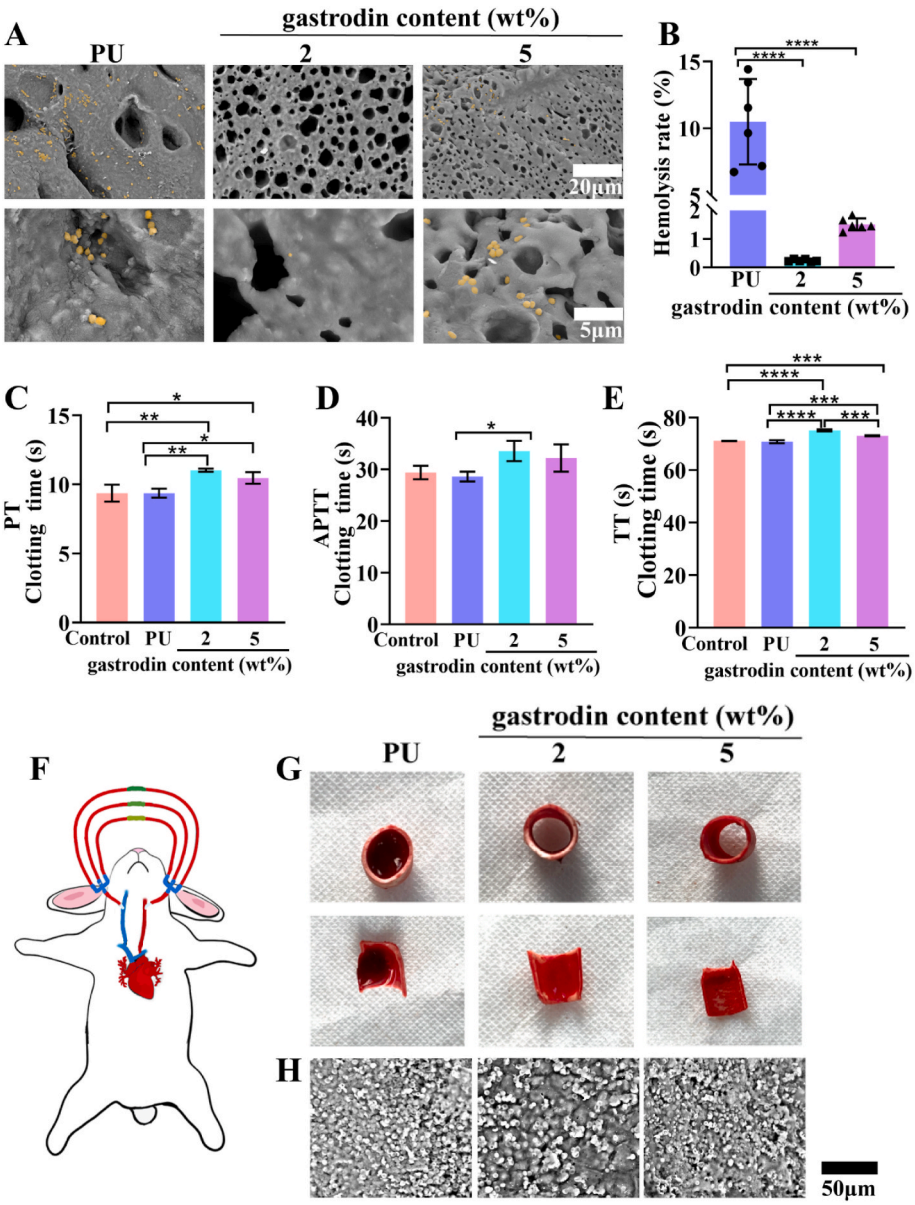


**Fig. 6.** Antithrombotic test of tri-phasic scaffolds *in vitro* and *ex vivo*. (**A**) SEM images of rabbit platelet-rich plasma (PRP) incubated with scaffolds. (**B**) The effect of scaffolds on hemolysis rate (n = 6). (**C**–**E**) Plasma coagulation time of PT (**C**), APTT (**D**), and TT (**E**) in the presence of scaffolds (n = 3). (**F**) The *ex vivo* extracorporeal blood circulation model of rabbit. (**G**) Photographs of thrombus on the scaffolds of PU, 2 and 5 wt% gastrodin-PU. (**H**) SEM images of adhered RBC. $^{****}P < 0.0001$, $^{***}P < 0.001$, $^{**}P < 0.01$ and $^{*}P < 0.05$ by one-way ANOVA with Tukey correction.

taken from PU was reduced from proximal (49.64 ± 17.319 %) and distant (61.04 ± 3.076 %) implantation, which reflected the high incidence of restenosis. Augmentative stenosis was also evident in 5 wt% gastrodin-PU group. As there was no more obstruction in 2 wt% gastrodin-PU group, the enhanced patency was more consistent with the result of ultrasound. After 3-month postoperation, 2 wt% gastrodin-PU group only showed a minimal stenosis, and the luminal diameter remained unchanged; however, there was serious thrombus lining the lumen of PU and 5 wt% gastrodin-PU groups.

In a longitudinal H&E image, cells from host could infiltrate gradually into the center of porous scaffolds (Fig. 7E). There was a significant amount of inner tissue covering the lumen of 2 wt% gastrodin-PU, yet only very minimal of it was observed in PU and 5 wt% gastrodin-PU groups at 4 weeks. Moreover, 2 wt% gastrodin-PU group showed advanced migration of a large amount of tissue into the center, and with time, the cell infiltration and tissue regeneration became most obvious among the three different groups. At week 12, after explantation, enhanced new tissues and enlarged porous structure were observed in 2 wt% gastrodin-PU group, preceding the other groups. The neointima thickness was sharply increased in PU and 5 wt% gastrodin-PU groups. The results with Masson's trichrome staining (Fig. S8) further confirmed that 2 wt% gastrodin-PU scaffold had the best patency and performance *in vivo* among the three different types of scaffolds.

Inflammatory microenvironment affects vascular regeneration and remodeling. Immunofluorescence staining revealed extensive overexpression of the M1 marker (TNF-α) but significantly lower expression of the M2 marker (Arg-1) by the macrophages in the PU group (Fig. 8A). Remarkably, in 2 wt% gastrodin-PU group, TNF-α expression was attenuated but expression of Arg-1 was enhanced when compared with the 5 wt% gastrodin-PU group. The results suggest that 2 wt% gastrodin-PU can partly suppress the M1 polarization; meanwhile, the alteration of the cellular microenvironment appears to promote M2 polarization during the regenerated process.

The endothelialization in the scaffold was followed till 12 weeks

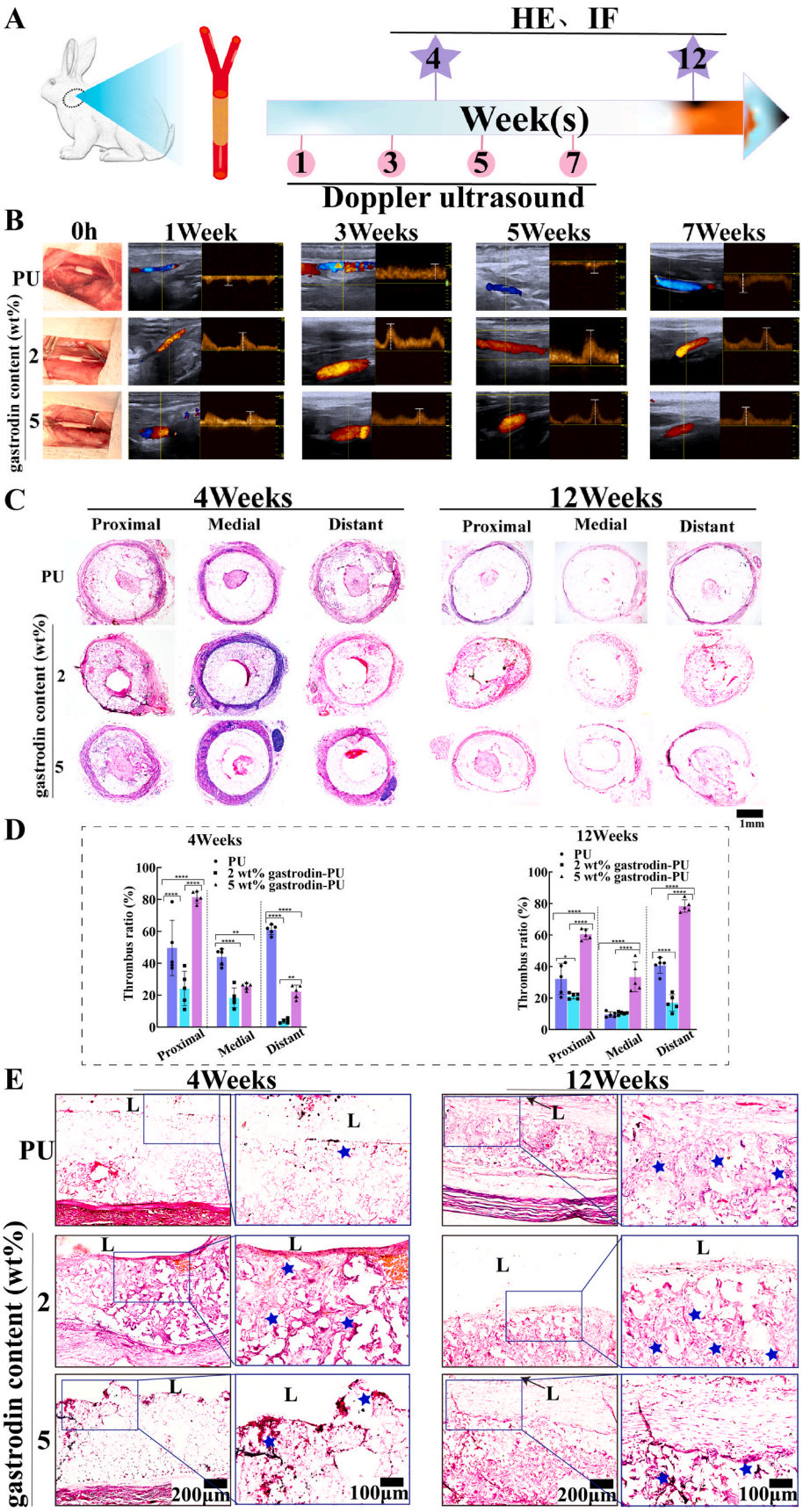


**Fig. 7.** Spatiotemporal delivery of gastrodin led to enhanced patency and neo-tissue infiltration after scaffold implantation. (**A**) Schematic representation of a rabbit carotid artery defect model establishment and following treatments. (**B**) Blood flow patency monitored by Doppler ultrasound. (**C**) H&E staining of cross-section. (**D**) Quantification of thrombus ratio (n = 5). (**E**) The longitudinal H&E images. L and star indicate the lumen and neo-tissue, respectively. $^{****}P < 0.0001$, $^{**}P < 0.01$ and $^{*}P < 0.05$ by one-way ANOVA with Tukey correction.

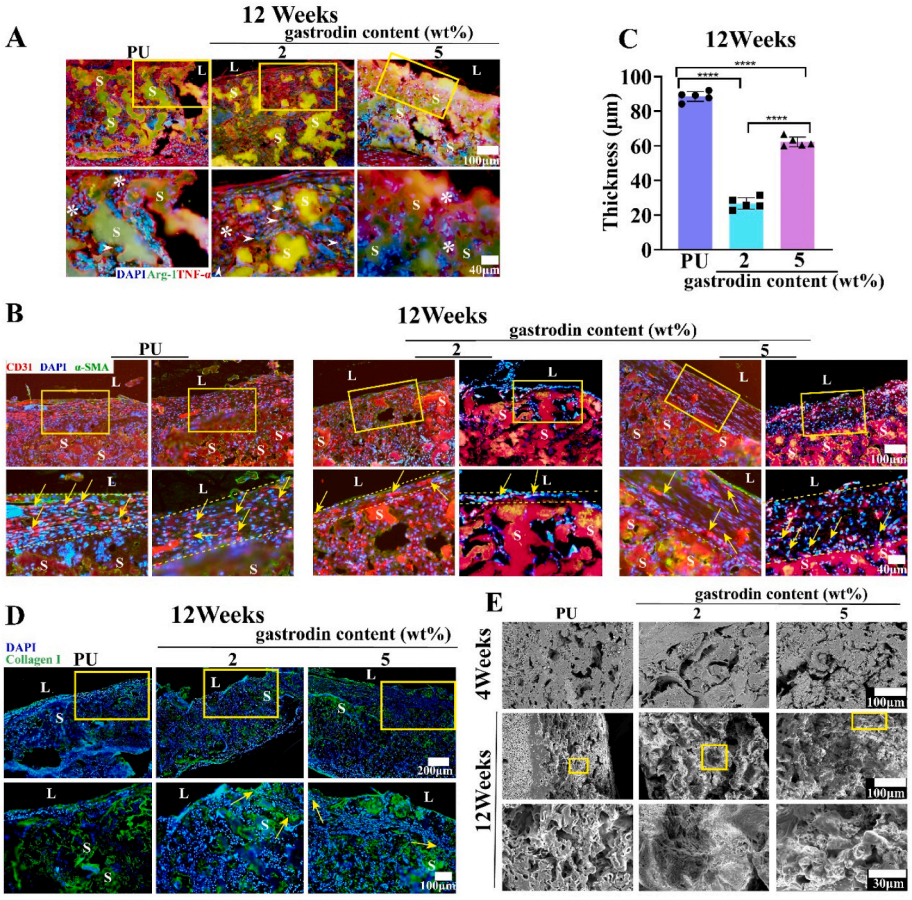


**Fig. 8.** *In vivo* regeneration evaluation on rabbit carotid artery model. (**A**) Anti-inflammatory properties by IF staining of Arg-1 (green, indicated by white arrows) and TNF-α (red, indicated by *) at 12 weeks. (**B**) Endothelialization of vascular scaffold at 12 weeks (red - CD31, green - α-SMA, blue - DAPI; yellow arrows indicate endothelial cells). (**C**) Quantitative analysis of endothelialization thickness (n = 5). (**D**) IF staining of collagen I (green, indicated by yellow arrows - collagen I, blue - DAPI). (**E**) The microstructure of tri-phasic scaffold after degradation *in vivo* by SEM. L and S indicate the lumen and scaffold, respectively. ****$P < 0.0001$ by one-way ANOVA with Tukey correction.

(Fig. 8B). It was found that the endothelial cells in the scaffolds of PU and 5 wt% gastrodin-PU groups grew significantly thicker, showing extensive hyperplasia of the intima. On the other hand, only a thin layer of endothelial cells spread over the surface in the 2 wt% gastrodin-PU scaffold (Fig. 8C). Concurrently, a larger number of smooth muscle cells (α-SMA) were observed to migrate inside the neointima of PU group in comparison with the other two groups. However, the incidence of smooth muscle cells in the 2 wt% gastrodin-PU group was less as compared to 5 wt% gastrodin-PU group, suggesting a better remodeling for 2 wt% gastrodin-PU scaffold. Type I collagen staining (Fig. 8D) showed that there was massive degradation of scaffolds and growth of type I collagen in the 2 wt% gastrodin-PU group, suggesting the presence of collagen and elastin fibers. In contrast, these features indicative of growth was evident in the 5 wt% gastrodin-PU group, and was even less significant in the PU group. SEM further confirmed only a moderate degree of degradability in the PU group (Fig. 8E). At 4 weeks, the micro-pores were enlarged, and the outer fibrous membrane of 2 wt% gastrodin-PU was obviously degraded than the others. The trends continued to 12 weeks, the 2 wt% gastrodin-PU group exhibited significantly increase in micro-pores and improved formed tissue resembling collagen I staining (Fig. 8D). At this time point, the outer fibers for all groups disappeared in line with the degradable properties *in vitro*. Thus, along with the inhibition of smooth muscle cell migration and proliferation as well as the antithrombogenesis, the intimal hyperplasia was effectively inhibited.

## 4. Discussion

After vascular interventions, anti-coagulation drugs are used to prevent platelet accumulation and thrombus formation. The results obtained in clinical trials for small diameter vascular blood vessels have not always shown the expected benefits to patients. The supra-physiological dosages of drugs needed to elicit a therapeutic effect and adverse effects attached to these high doses are common and there have hampered their application [31,32]. It has been reported that appropriate patterning of gastrodin can inhibit SMC proliferation [24], and attenuate neointimal hyperplasia in response to vascular injury [15,33]. Gastrodin also exerts vasorelaxation effect through activation of protein kinase A (PKA) and subsequent opening of smooth muscle $K_{ATP}$ channels, and this effect was independent of endothelium [34]. We reported previously that gastrodin-release PU facilitates HUVECs coverage and blood vessel formation which would affect endothelialization of inner layer [20]. Although we had developed a gastrodin-release system with the degradation of polyurethane, its simple delivery was not sufficient for a complex process. It is imperative when distinctively regulating hierarchical tissue regeneration that drug dosages can be adapted to multi-hierarchical structures to precisely regulate the fate of different cells. To this end, the present study has presented an alternative strategy for spatiotemporally controlled delivery of gastrodin to meet the needs of different cell cascades. We developed a range of gastrodin-functionalized polyurethanes, constructing small diameter vascular scaffolds with bi-phasic pore structure by changing the pore-forming particle size in dipping solutions without the need of

altering the material chemistry. The inner layer had significantly smaller pores and thinner wall thickness compared to medial layers, which were fabricated with pore-forming particles mixture (Fig. 1B). The outer layer was fibrous PCL whose periphery location making it a promising support for bi-phasic structure from collapsing or sagging. The inner layer showed a fast gastrodin release, while the addition of pore-forming particles to the medial layer was found to have a significant effect on both degradable rate and release of gastrodin (Fig. 1I and J and K). In the latter, the pore-forming particles reduced at least partially the gastrodin content per unit volume, thus resulting in a slower and lesser gastrodin release. In addition, release rate of gastrodin in inner layer was rapid at initial stage and then tended to slow down, while a slow upward trend appeared in medial layer (Fig. S6). The constructs containing spatio-temporal gradients of gastrodin allowed for controlled hierarchical tissue regeneration with suitable dosages.

Scaffolds with proper compliance (Fig. 1E and F) and smooth inner surface (Fig. 1D) would decrease localized flow disturbance, leading to the patency of lumen. The *ex vivo* extracorporeal blood circulation experiment showed positive antithrombogenic effects due to gastrodin incorporated in the context of materials implanted directly into the vasculature. Very strikingly, very little platelets appeared on the surface of gastrodin-PU scaffolds and the prolonged clotting times were directly dependent upon gastrodin-releasing over the inner layers (Fig. 6). We used the rabbit right common carotid artery model to study the effect of gastrodin-releasing on scaffold patency *in vivo*. Although the gastrodin content was variable, all scaffolds maintained sufficient burst pressure to withstand the physiological blood pressure (Fig. 1G) during implantation. Of note, the 2 wt% gastrodin-PU showed a higher 1-month patency rate, stronger blood flow and reduced intimal hyperplasia area compared to the PU scaffold (Figs. 7B and 8, B and C). Quantitative thrombus ratio of lumens showed that 2 wt% gastrodin-PU scaffold was lower than the PU and 5 wt% gastrodin-PU scaffolds and remained to be consistent from week 4 to week 12 (Fig. 7C and D). Moreover, the data of color Doppler ultrasound confirmed a better outcome of gastrodin-modified scaffolds, because gastrodin significantly improved the patency rate of scaffolds throughout 12 weeks post-implantation (Fig. 7B). Liu et al. had also reported that gastrodin possessed the property of anti-coagulation, and that the underlying mechanism for this was by interfering with the interaction between fibrins [35].

In addition to the antiplatelet and antithrombogenic ability, the effect of dual-functional structure on smooth muscle cell inhibition and endothelial cell promotion is also important because of its correlation to neointimal hyperplasia and endothelial regeneration [36–38]. Usually, graft implantation causes endothelium damage, which inevitably lead to the leak of smooth muscle cells, thus endothelial cells would directly compete with smooth muscle cells [39]. Intimal hyperplasia formation is related with smooth muscle cell migration, proliferation, secretion of extracellular matrix, and phenotype changes of smooth muscle cell from contractile to synthetic phenotype [40,41]. To exert more precise control over key factors in intimal endothelial cells and medial smooth muscle cells and to drive endothelial cells settle precisely while avoiding hyperplasia concerns associated with smooth muscle cell invasion, we have used small sized pores to form physical shields against the smooth muscle cells. When cultured with SMCs, gastrodin-PU promoted SMC phenotypic switching, as indicated by decreased proliferation/migration and increased SMC contractile proteins. In contrast, 2 wt% gastrodin-PU increased α-SMA (or calponin) and osteopontin expression, and the contractile protein α-SMA was slightly better than osteopontin (Fig. 2). It is intriguing that osteopontin, a marker of synthetic smooth muscle cells, was remarkedly decreased in 2 wt% gastrodin-PU group when treated with conditioned medium of HUVECs-inner layer. This may be attributed to the regulatory effect of HUVEC-inner layer on the SMCs (Fig. 4D). When treated with conditioned medium of SMC-medial layer, migration of HUVECs showed no significant difference (Fig. 4A). In histological stained sections, collagen and smooth fibers in the lumen of 2 wt% gastrodin-PU scaffold were slightly more but not significant when compared with that of PU scaffold (Fig. 8D). We further observed more intense α-SMA expression in the neointima section of most PU and 5 wt% gastrodin-PU scaffolds compared to 2 wt% gastrodin-PU scaffold (Fig. 8, B and D). Together, the inhibitory effect of scaffold on SMCs benefits from its inherent inhibition of SMC proliferation by gastrodin loaded into the medial layer, as well as the regulation of HUVEC-inner layer.

Under the condition without the control of endothelial cells, excessive smooth muscle cell growth and delayed re-endothelialization on the surface of grafts will result in hyperplasia and in-stent restenosis [42]. The early staged formation of endothelial cell coverage on the luminal surface of grafts has been essential for successful grafting. However, graft implantation can provoke an innate immune response inducing a pro-inflammatory environment which could result in chronic inflammation leading to an impaired vascular regeneration [43]. Unfavorable inflammatory factors damage endothelial cells, causing and exacerbating subsequent intimal hyperplasia and inadequate endothelialization of grafts. Thus, shifting a pro-inflammatory environment towards an anti-inflammatory one upon graft implantation has been considered another key process for a favoring tissue restoration. Macrophages have been shown to closely associate with immunomodulation and angiogenesis, releasing various cellular contents including pro-healing cytokines and growth factors which further protect cells or tissues from inflammatory damage and to promote survival [44,45]. Gastrodin-release materials can stimulate macrophages to polarize into M2 anti-inflammatory property in the tissue remodeling process [46]. In this study, we also observed the anti-inflammatory performance of the gastrodin-modified scaffolds *in vivo*. At 4 and 12 weeks, there was more severe inflammatory cell infiltration in the PU group. In contrast, a milder inflammation was found within the 2 wt% gastrodin-PU scaffold, as manifested by the presence of a distinct anti-inflammatory phenotype (Arg-1-M2); conversely, more pro-inflammatory phenotypes (TNF-α-M1) were found within the PU group (fig. S9 and Fig. 8A). Antagonism of TNF-α has been previously linked to similar endothelial protective effects [47]. These effects potentially supported the enhanced re-endothelialization of 2 wt% gastrodin-PU scaffold compared to PU and 5 wt% gastrodin-PU scaffolds. Here, gastrodin-releasing ability that provides a biomimetic microenvironment with HUVEC-preferred properties was be seen when HUVECs were cultured with inner layer *in vitro* (Fig. 3). Further endothelial coverage was found in the inner layer and only achieved baseline levels of re-endothelialization *in vivo*. After 12-week implantation, CD31 immunofluorescence was detected on the abluminal surface of explanted scaffolds, indicating that more visual capillary formations were formed in the 2 wt% gastrodin-PU group (Fig. 8B). Collagen-I immunofluorescence staining demonstrated that some matrix was deposited within the scaffold walls (Fig. 8D). This would promote hierarchical tissue regeneration which was accompanied by obvious degradability as shown by SEM (Fig. 8E). On the other hand, both PU and 5 wt% gastrodin-PU groups showed more obvious intima thickening compared with 2 wt% gastrodin-PU at week 12, indicating more active proliferation and migration of SMCs.

The limited proliferation and migration of SMCs were probably associated with increased eNOS expression in both gastrodin-PU groups. A key function of eNOS molecule is the promotion of endothelialization at the vascular lesion sites and on the stent surfaces [48,49]. The 2 wt% gastrodin-PU scaffold not only had the highest levels of endothelial coverage by inducing VEGF and VE-cadherin expression (Fig. 3), but also enhanced early eNOS expression compared to others (Fig. 5G and H). Although the 5 wt% gastrodin-PU also exhibited potent eNOS expression, its inhibitory effect on SMCs was still weaker than the 2 wt% gastrodin-PU group (Fig. 4, A and D). Consistent with our research, precious studies also showed that thrombosis and neointimal proliferation were significantly inhibited with eNOS [50,51]. The endothelium-mimic NO levels are conducive to endothelialized functions and synergetically inhibited thrombogenesis in a vascular microenvironment [52]. HSP70 is a well-known protective protein for

adequate vascular reactivity [24,53], which was extensively expressed in response to gastrodin-PU groups. We are confident that regulation process between HUVECs and SMCs mediated by relevant layers activates eNOS and HSP70 signal, thus inhibiting SMC proliferation [54]. A competition experiment between HUVECs and SMCs intervened with distinct layers further confirmed that the collective anti-proliferative effects were greatest impact to SMCs, highlighting safety limitations between SMCs and HUVECs in promoting vessel healing and decreasing risk of thrombosis (Fig. 4). The 2 wt% gastrodin-PU scaffold could provide HUVEC-friendly biological activity to elicit enhanced HUVEC proliferation and migration against those of the SMCs. In other words, this study justified the superiority of a spatiotemporal gastrodin and structure for the inhibition SMC-caused intimal hyperplasia and in situ generation of a pure endothelium *in vivo*. The limitations of the study lie in the lack of accurate categorization and control for spatiotemporal structure, which might further help identify the precise regeneration of hierarchical tissue. Further study should investigate the competitive regulation mechanism between HUVECs and SMCs mediated by spatiotemporal gastrodin construct.

## 5. Conclusions

This study fabricated a range of tri-phasic scaffolds with spatiotemporally defined structure and gastrodin-release for small-diameter vascular grafts. While the small pores of inner layer provided topographic guidance for infiltration of HUVECs, the bigger pores of medial layer could offer SMC-friendly habitat. Spatial distribution and differential regulation of key proteins in HUVECs and SMCs were mediated by hierarchical release of gastrodin, of which rapid release in inner layer elicited enhanced HUVEC proliferation and migration against those of the SMC. Further, when treated with conditioned media of SMC-medial layer incubation, HUVECs progressed in proliferation, but the migration was not affected. In contrast, the inhibition of SMC migration and proliferation was achieved by introducing conditioned media of HUVEC-inner layer incubation, which may activate eNOS and HSP70 signal. *In vivo* examination further corroborated hierarchical vascular regeneration and maintained high patency. Overall, the benefit of gastrodin localization in both time and space is tightly controlled growth of the intima and media, thereby hastening hierarchical vascular regeneration.

## Data availability statement

The data that support the findings of this study are available from the corresponding author upon reasonable request.

## Ethics approval and consent to participate

The reported work follows the guidelines approved by the Institutional Animal Care and Use Committee of Kunming Medical University (China). All of the authors consented to participate in the reported work.

## CRediT authorship contribution statement

**Yingrui Hu:** Visualization, Investigation, Data curation. **Limei Li:** Writing – original draft, Investigation, Formal analysis, Conceptualization. **Qing Li:** Investigation. **Shilin Pan:** Investigation. **Guangli Feng:** Investigation. **Xiaoqian Lan:** Investigation. **Jianlin Jiao:** Investigation. **Lianmei Zhong:** Supervision, Resources, Conceptualization. **Lin Sun:** Writing – review & editing, Supervision, Resources, Conceptualization.

## Declaration of competing interest

The authors declare that they have no known competing financial interests or personal relationships that could have appeared to influence the work reported in this paper.

## Acknowledgments

This project was funded by National Natural Science Foundation of China (grant no. 82260088, 81960251, 82260366), Yunnan Provincial Innovative Research Team in Basic and Clinical Study of Coronary Heart Disease of Yunnan Revitalization Talent Support Program (202305AS350030), Yunnan Science and Technology Program (202401AY070001-030, 202201AT070136, 202301AY070001-032, 202001AY070001-014), Bai Xiaochun expert workstation (YSZJGZZ-2020040).

## Appendix A. Supplementary data

Supplementary data to this article can be found online at https://doi.org/10.1016/j.bioactmat.2024.05.007.

## References

[1] J. Hou, X. Zhang, Y. Wu, J. Jie, Z. Wang, G.-Q. Chen, J. Sun, L.-P. Wu, Amphiphilic and fatigue-resistant organohydrogels for small-diameter vascular grafts, Sci. Adv. 8 (2022) eabn5360, https://doi.org/10.1126/sciadv.abn5360.
[2] A.P. Rickel, X. Deng, D. Engebretson, Z. Hong, Electrospun nanofiber scaffold for vascular tissue engineering, Mater. Sci. Eng., C 129 (2021) 112373, https://doi.org/10.1016/j.msec.2021.112373.
[3] Z. Zhu, Q. Gao, Z. Long, Q. Huo, Y. Ge, N. Vianney, N.A. Daliko, Y. Meng, J. Qu, H. Chen, B. Wang, Polydopamine/poly(sulfobetaine methacrylate) Co-deposition coatings triggered by CuSO(4)/H(2)O(2) on implants for improved surface hemocompatibility and antibacterial activity, Bioact. Mater. 6 (2021) 2546–2556, https://doi.org/10.1016/j.bioactmat.2021.01.025.
[4] T. Melnik, O. Jordan, J.-M. Corpataux, F. Delie, F. Saucy, Pharmacological prevention of intimal hyperplasia: a state-of-the-art review, Pharmacol. Therapeut. 235 (2022) 108157, https://doi.org/10.1016/j.pharmthera.2022.108157.
[5] H. Ullrich, M. Olschewski, T. Münzel, T. Gori, Coronary in-stent restenosis: predictors and treatment, Deutsches Arzteblatt Int. 118 (2021) 637–644, https://doi.org/10.3238/arztebl.m2021.0254.
[6] J. Greenhalgh, J. Hockenhull, N. Rao, Y. Dundar, R.C. Dickson, A. Bagust, Drug-eluting stents versus bare metal stents for angina or acute coronary syndromes, Cochrane Database Syst. Rev. (2010) CD004587, https://doi.org/10.1002/14651858.CD004587.pub2.
[7] M. Vila Cuenca, A. Cochrane, F.E. van den Hil, A.A.F. de Vries, S.A.J. Lesnik Oberstein, C.L. Mummery, V. V Orlova, Engineered 3D vessel-on-chip using hiPSC-derived endothelial- and vascular smooth muscle cells, Stem Cell Rep. 16 (2021) 2159–2168, https://doi.org/10.1016/j.stemcr.2021.08.003.
[8] X. Li, L. Huang, L. Li, Y. Tang, Q. Liu, H. Xie, J. Tian, S. Zhou, G. Tang, Biomimetic dual-oriented/bilayered electrospun scaffold for vascular tissue engineering, J. Biomater. Sci. Polym. Ed. 31 (2020) 439–455, https://doi.org/10.1080/09205063.2019.1697171.
[9] J.L. Hernandez, K.A. Woodrow, Medical applications of porous biomaterials: features of porosity and tissue-specific implications for biocompatibility, Adv. Healthcare Mater. 11 (2022) e2102087, https://doi.org/10.1002/adhm.202102087.
[10] I.S. Park, S.-H. Kim, Y.H. Kim, I.H. Kim, S.H. Kim, A collagen/smooth muscle cell-incorporated elastic scaffold for tissue-engineered vascular grafts, J. Biomater. Sci. Polym. Ed. 20 (2009) 1645–1660, https://doi.org/10.1163/156856208X386237.
[11] Y. Yang, D. Lei, H. Zou, S. Huang, Q. Yang, S. Li, F.-L. Qing, X. Ye, Z. You, Q. Zhao, Hybrid electrospun rapamycin-loaded small-diameter decellularized vascular grafts effectively inhibit intimal hyperplasia, Acta Biomater. 97 (2019) 321–332, https://doi.org/10.1016/j.actbio.2019.06.037.
[12] J. Fu, M. Wang, I. De Vlaminck, Y. Wang, Thick PCL fibers improving host remodeling of PGS-PCL composite grafts implanted in rat common carotid arteries, Small 16 (2020) e2004133, https://doi.org/10.1002/smll.202004133.
[13] Z. Zeng, C. Hu, Q. Liang, L. Tang, D. Cheng, C. Ruan, Coaxial-printed small-diameter polyelectrolyte-based tubes with an electrostatic self-assembly of heparin and YIGSR peptide for antithrombogenicity and endothelialization, Bioact. Mater. 6 (2021) 1628–1638, https://doi.org/10.1016/j.bioactmat.2020.10.028.
[14] H. Warner, Y. Wu, W.D. Wagner, Syndecan-4 functionalization of tissue regeneration scaffolds improves interaction with endothelial progenitor cells, Regen. Biomater. 8 (2021) rbab070, https://doi.org/10.1093/rb/rbab070.
[15] L. Zhu, H. Guan, C. Cui, S. Tian, D. Yang, X. Wang, S. Zhang, L. Wang, H. Jiang, Gastrodin inhibits cell proliferation in vascular smooth muscle cells and attenuates neointima formation in vivo, Int. J. Mol. Med. 30 (2012) 1034–1040, https://doi.org/10.3892/ijmm.2012.1100.
[16] A. Kurane, N. Vyavahare, In vivo vascular tissue engineering: influence of cytokine and implant location on tissue specific cellular recruitment, J. Tissue Eng. Regen. Med. 3 (2009) 280–289, https://doi.org/10.1002/term.164.
[17] L. Li, Q. Li, L. Gui, Y. Deng, L. Wang, J. Jiao, Y. Hu, X. Lan, J. Hou, Y. Li, D. Lu, Sequential gastrodin release PU/n-HA composite scaffolds reprogram macrophages for improved osteogenesis and angiogenesis, Bioact. Mater. 19 (2023) 24–37, https://doi.org/10.1016/j.bioactmat.2022.03.037.
[18] G. Xiao, R. Tang, N. Yang, Y. Chen, Review on pharmacological effects of gastrodin, Arch Pharm. Res. (Seoul) (2023), https://doi.org/10.1007/s12272-023-01463-0.

[19] J. Tao, P. Yang, L. Xie, Y. Pu, J. Guo, J. Jiao, L. Sun, D. Lu, Gastrodin induces lysosomal biogenesis and autophagy to prevent the formation of foam cells via AMPK-FoxO1-TFEB signalling axis, J. Cell Mol. Med. 25 (2021) 5769–5781, https://doi.org/10.1111/jcmm.16600.
[20] M. Zheng, J. Guo, Q. Li, J. Yang, Y. Han, H. Yang, M. Yu, L. Zhong, D. Lu, L. Li, L. Sun, Syntheses and characterization of anti-thrombotic and anti-oxidative Gastrodin-modified polyurethane for vascular tissue engineering, Bioact. Mater. 6 (2021) 404–419, https://doi.org/10.1016/j.bioactmat.2020.08.008.
[21] J. Wang, M. Wu, The up-regulation of miR-21 by gastrodin to promote the angiogenesis ability of human umbilical vein endothelial cells by activating the signaling pathway of PI3K/Akt, Bioengineered 12 (2021) 5402–5410, https://doi.org/10.1080/21655979.2021.1964895.
[22] S. Wendels, L. Avérous, Biobased polyurethanes for biomedical applications, Bioact. Mater. 6 (2021) 1083–1106, https://doi.org/10.1016/j.bioactmat.2020.10.002.
[23] C. Xu, Y. Hong, Rational design of biodegradable thermoplastic polyurethanes for tissue repair, Bioact. Mater. 15 (2022) 250–271, https://doi.org/10.1016/j.bioactmat.2021.11.029.
[24] A. Shen, M. Wu, F. Ali, Z. Guo, Y. Fang, Y. Zhou, S. Zhang, W. Zhang, Y. Wen, M. Yu, J. Peng, K. Chen, Based on network pharmacology, gastrodin attenuates hypertension-induced vascular smooth muscle cell proliferation and PI3K/AKT pathway activation, Sci. Rep. 13 (2023) 12140, https://doi.org/10.1038/s41598-023-39202-6.
[25] U. Rykaczewska, B.E. Suur, S. Röhl, A. Razuvaev, M. Lengquist, M. Sabater-Lleal, S. W. van der Laan, C.L. Miller, R.C. Wirka, M. Kronqvist, M. Gonzalez Diez, M. Vesterlund, P. Gillgren, J. Odeberg, J.H. Lindeman, F. Veglia, S.E. Humphries, U. de Faire, D. Baldassarre, E. Tremoli, J. Lehtiö, G.K. Hansson, G. Paulsson-Berne, G. Pasterkamp, T. Quertermous, A. Hamsten, P. Eriksson, U. Hedin, L. Matic, PCSK6 is a key protease in the control of smooth muscle cell function in vascular remodeling, Circ. Res. 126 (2020) 571–585, https://doi.org/10.1161/CIRCRESAHA.119.316063.
[26] K. Miyagawa, M. Shi, P.I. Chen, J.K. Hennigs, Z. Zhao, M. Wang, C.G. Li, T. Saito, S. Taylor, S. Sa, A. Cao, L. Wang, M.P. Snyder, M. Rabinovitch, Smooth muscle contact drives endothelial regeneration by BMPR2-Notch1-Mediated metabolic and epigenetic changes, Circ. Res. 124 (2019) 211–224, https://doi.org/10.1161/CIRCRESAHA.118.313374.
[27] M. Bouchet, M. Gauthier, M. Maire, A. Ajji, S. Lerouge, Towards compliant small-diameter vascular grafts: predictive analytical model and experiments, Mater. Sci. Eng., C 100 (2019) 715–723, https://doi.org/10.1016/j.msec.2019.03.023.
[28] L.R. Versteegden, K.A. van Kampen, H.P. Janke, D.M. Tiemessen, H. R. Hoogenkamp, T.G. Hafmans, E.A. Roozen, R.M. Lomme, H. van Goor, E. Oosterwijk, W.F. Feitz, T.H. van Kuppevelt, W.F. Daamen, Tubular collagen scaffolds with radial elasticity for hollow organ regeneration, Acta Biomater. 52 (2017) 1–8, https://doi.org/10.1016/j.actbio.2017.02.005.
[29] N. Wang, W. Zheng, S. Cheng, W. Zhang, S. Liu, X. Jiang, In vitro evaluation of essential mechanical properties and cell behaviors of a novel polylactic-co-glycolic acid (PLGA)-based tubular scaffold for small-diameter vascular tissue engineering, Polymers 9 (2017), https://doi.org/10.3390/polym9080318.
[30] D. Zhu, I. Cockerill, Y. Su, Z. Zhang, J. Fu, K.-W. Lee, J. Ma, C. Okpokwasili, L. Tang, Y. Zheng, Y.-X. Qin, Y. Wang, Mechanical strength, biodegradation, and in vitro and in vivo biocompatibility of Zn biomaterials, ACS Appl. Mater. Interfaces 11 (2019) 6809–6819, https://doi.org/10.1021/acsami.8b20634.
[31] J. Fanikos, Y. Tawfik, D. Almheiri, K. Sylvester, L.F. Buckley, C. Dew, H. Dell'Orfano, A. Armero, A. Bejjani, B. Bikdeli, U. Campia, J. Davies, K. Fiumara, H. Hogan, C.D. Khairani, D. Krishnathasan, J. Lou, A. Makawi, R.H. Morrison, N. Porio, A. Tristani, J.M. Connors, S.Z. Goldhaber, G. Piazza, Anticoagulation-associated adverse drug events in hospitalized patients across two time periods, Am. J. Med. 136 (2023), https://doi.org/10.1016/j.amjmed.2023.05.013.
[32] Y. Ozaki, A.G. Violaris, P.W. Serruys, New stent technologies, Prog. Cardiovasc. Dis. 39 (1996) 129–140. https://pubmed.ncbi.nlm.nih.gov/8841007.
[33] P. Yang, Y. Han, L. Gui, J. Sun, Y. Chen, R. Song, J. Guo, Y. Xie, D. Lu, L. Sun, Gastrodin attenuation of the inflammatory response in H9c2 cardiomyocytes involves inhibition of NF-κB and MAPKs activation via the phosphatidylinositol 3-kinase signaling, Biochem. Pharmacol. 85 (2013) 1124–1133, https://doi.org/10.1016/j.bcp.2013.01.020.
[34] S. Chen, X. Hao, L. Yu, P. Zhang, W. Cao, H. Chen, D. Zhu, Gastrodin causes vasodilation by activating KATP channels in vascular smooth muscles via PKA-dependent signaling pathway, J. Recept. Signal Transduct. Res. 37 (2017) 543–549, https://doi.org/10.1080/10799893.2017.1369118.
[35] Y. Liu, X. Tang, J. Pei, L. Zhang, F. Liu, K. Li, Gastrodin interaction with human fibrinogen: anticoagulant effects and binding studies, Chemistry (Weinheim an Der Bergstrasse, Germany) 12 (2006) 7807–7815. https://pubmed.ncbi.nlm.nih.gov/16847996.
[36] T. Wu, C. Huang, D. Li, A. Yin, W. Liu, J. Wang, J. Chen, H. Ei-Hamshary, S.S. Al-Deyab, X. Mo, A multi-layered vascular scaffold with symmetrical structure by bi-directional gradient electrospinning, Colloids Surf. B Biointerfaces 133 (2015) 179–188, https://doi.org/10.1016/j.colsurfb.2015.05.048.
[37] T. Wu, J. Zhang, Y. Wang, B. Sun, M. Yin, G.L. Bowlin, X. Mo, Design and fabrication of a biomimetic vascular scaffold promoting in situ endothelialization and tunica media regeneration, ACS Appl. Bio Mater. 1 (2018) 833–844, https://doi.org/10.1021/acsabm.8b00269.
[38] P. Li, F. Liang, L. Wang, D. Jin, Y. Shang, X. Liu, Y. Pan, J. Yuan, J. Shen, M. Yin, Bilayer vascular grafts with on-demand NO and H2S release capabilities, Bioact. Mater. 31 (2024) 38–52, https://doi.org/10.1016/j.bioactmat.2023.07.020.
[39] M.H. Kural, J. Wang, L. Gui, Y. Yuan, G. Li, K.L. Leiby, E. Quijano, G. Tellides, W. M. Saltzman, L.E. Niklason, Fas ligand and nitric oxide combination to control smooth muscle growth while sparing endothelium, Biomaterials 212 (2019) 28–38, https://doi.org/10.1016/j.biomaterials.2019.05.011.
[40] Z. Zeng, L. Xia, S. Fan, J. Zheng, J. Qin, X. Fan, Y. Liu, J. Tao, Y. Liu, K. Li, Z. Ling, Y. Bu, K.A. Martin, J. Hwa, R. Liu, W.H. Tang, Circular RNA circMAP3K5 acts as a microRNA-22-3p sponge to promote resolution of intimal hyperplasia via TET2-Mediated smooth muscle cell differentiation, Circulation 143 (2021) 354–371, https://doi.org/10.1161/CIRCULATIONAHA.120.049715.
[41] R. Chakraborty, F.Z. Saddouk, A.C. Carrao, D.S. Krause, D.M. Greif, K.A. Martin, Promoters to study vascular smooth muscle, Arterioscler. Thromb. Vasc. Biol. 39 (2019) 603–612, https://doi.org/10.1161/ATVBAHA.119.312449.
[42] R. Wang, J. Lu, J. Yin, H. Chen, H. Liu, F. Xu, T. Zang, R. Xu, C. Li, Y. Wu, Q. Wu, X. Fei, M. Zhu, L. Shen, J. Ge, A TEMPOL and rapamycin loaded nanofiber-covered stent favors endothelialization and mitigates neointimal hyperplasia and local inflammation, Bioact. Mater. 19 (2023) 666–677, https://doi.org/10.1016/j.bioactmat.2022.04.033.
[43] L. Wang, X. Wei, Y. Wang, Promoting angiogenesis using immune cells for tissue-engineered vascular grafts, Ann. Biomed. Eng. 51 (2023) 660–678, https://doi.org/10.1007/s10439-023-03158-5.
[44] H. Hong, X.Y. Tian, The role of macrophages in vascular repair and regeneration after ischemic injury, Int. J. Mol. Sci. 21 (2020), https://doi.org/10.3390/ijms21176328.
[45] Z. Luo, W. Peng, Y. Xu, Y. Xie, Y. Liu, H. Lu, Y. Cao, J. Hu, Exosomal OTULIN from M2 macrophages promotes the recovery of spinal cord injuries via stimulating Wnt/β-catenin pathway-mediated vascular regeneration, Acta Biomater. 136 (2021) 519–532, https://doi.org/10.1016/j.actbio.2021.09.026.
[46] J. Jia, X. Shi, X. Jing, J. Li, J. Gao, M. Liu, C.-I. Lin, X. Guo, Q. Hua, BCL6 mediates the effects of Gastrodin on promoting M2-like macrophage polarization and protecting against oxidative stress-induced apoptosis and cell death in macrophages, Biochem. Biophys. Res. Commun. 486 (2017) 458–464, https://doi.org/10.1016/j.bbrc.2017.03.062.
[47] X. Hou, S. Yang, J. Yin, Blocking the REDD1/TXNIP axis ameliorates LPS-induced vascular endothelial cell injury through repressing oxidative stress and apoptosis, Am. J. Physiol. Cell Physiol. 316 (2019) C104–C110, https://doi.org/10.1152/ajpcell.00313.2018.
[48] N. Parsamanesh, A. Asghari, S. Sardari, A. Tasbandi, T. Jamialahmadi, S. Xu, A. Sahebkar, Resveratrol and endothelial function: a literature review, Pharmacol. Res. 170 (2021) 105725, https://doi.org/10.1016/j.phrs.2021.105725.
[49] M. Siragusa, I. Fleming, The eNOS signalosome and its link to endothelial dysfunction, Pflueg. Arch. Eur. J. Physiol. 468 (2016) 1125–1137, https://doi.org/10.1007/s00424-016-1839-0.
[50] G.-H. Lee, T.-H. Hoang, E.-S. Jung, S.-J. Jung, S.-K. Han, M.-J. Chung, S.-W. Chae, H.-J. Chae, Anthocyanins attenuate endothelial dysfunction through regulation of uncoupling of nitric oxide synthase in aged rats, Aging Cell 19 (2020) e13279, https://doi.org/10.1111/acel.13279.
[51] O. Porembskaya, Y. Toropova, V. Tomson, K. Lobastov, L. Laberko, V. Kravchuk, S. Saiganov, A. Brill, Pulmonary artery thrombosis: a diagnosis that strives for its independence, Int. J. Mol. Sci. 21 (2020), https://doi.org/10.3390/ijms21145086.
[52] N. Lyu, Z. Du, H. Qiu, P. Gao, Q. Yao, K. Xiong, Q. Tu, X. Li, B. Chen, M. Wang, G. Pan, N. Huang, Z. Yang, Mimicking the nitric oxide-releasing and glycocalyx functions of endothelium on vascular stent surfaces, Adv. Sci. 7 (2020) 1–12, https://doi.org/10.1002/advs.202002330.
[53] S.L. Park, T.-W. Chung, S. Kim, B. Hwang, J.M. Kim, H.M. Lee, H.-J. Cha, Y. Seo, S. Y. Choe, K.-T. Ha, G. Kim, S.-J. Yun, S.-S. Park, Y.H. Choi, B.K. Kim, W.-T. Kim, E.-J. Cha, C. Patterson, W.-J. Kim, S.-K. Moon, HSP70-1 is required for interleukin-5-induced angiogenic responses through eNOS pathway, Sci. Rep. 7 (2017) 44687, https://doi.org/10.1038/srep44687.
[54] K.J.A. McCullagh, R. Cooney, T. O'Brien, Endothelial nitric oxide synthase induces heat shock protein HSPA6 (HSP70B') in human arterial smooth muscle cells, Nitric Oxide: Bio. Chem. 52 (2016) 41–48, https://doi.org/10.1016/j.niox.2015.11.002.